
RF Project 765327/718226
Final Report

NASA-CR-183159
19880017789

AN EXPERIMENTAL STUDY OF THE EFFECT OF PITCH RATE
ON DELTA WING AERODYNAMICS AND STABILITY

M.B. Bragg
Aeronautical and Astronautical Research Laboratory

For the Period
April 1, 1986 - June 30, 1988

NATIONAL AERONAUTICS AND SPACE ADMINISTRATION
Langley Research Center
Hampton, Virginia 23665

Grant No. NAG-1-641

August 1988



**The Ohio State University
Research Foundation**

1314 Kinnear Road
Columbus, Ohio 43212



NF00248



Aeronautical and Astronautical
Research Laboratory

2300 West Case Road
Columbus, OH 43235-1919
Phone 614-292-5491

FINAL REPORT

NASA GRANT NAG-1-641 (RF 718226)

AN EXPERIMENTAL STUDY OF THE EFFECT OF PITCH
RATE ON DELTA WING AERODYNAMICS AND STABILITY

M. B. BRAGG
THE OHIO STATE UNIVERSITY
COLUMBUS, OHIO

AUGUST 1988

N88-27175#

FINAL REPORT: NAG-1-641

The final report for the research conducted under this grant are contained in two documents attached. The first document, in Appendix A, is a copy of a presentation made to NASA Langley personnel, December 10, 1987. This report briefly presents an initial analysis of the experiments. The second document, Appendix B, is a copy of an AIAA paper given in June 1988. This paper describes in detail the test set-up, data acquisition and reduction, and the results obtained. As agreed to with the NASA Langley technical managers of this research program, this paper serves as the primary final report document for this grant.

APPENDIX A



Aeronautical and Astronautical
Research Laboratory

2300 West Case Road
Columbus, OH 43220-1949
Phone 614-292-5491

**EXPERIMENTAL MEASUREMENTS ON AN OSCILLATING
70-DEGREE DELTA WING IN SUBSONIC FLOW**

M. R. Soltani* and M. B. Bragg
THE OHIO STATE UNIVERSITY
Columbus, Ohio**

and

**J. M. Brandon†
NASA LANGLEY RESEARCH CENTER
Hampton, Virginia**

PAPER NO. 88-2576

**AIAA 6th APPLIED AERODYNAMICS CONFERENCE
June 6-8, 1988
Williamsburg, VA**

***Graduate Research Assistant, Department of
Aeronautical & Astronautical Engineering,
Member AIAA**

****Associate Professor, Department of
Aeronautical & Astronautical Engineering,
Senior Member AIAA**

**†Aerospace Engineer, Flight Dynamics Branch,
Member, AIAA**

EXPERIMENTAL MEASUREMENTS ON AN OSCILLATING
70-DEGREE DELTA WING IN SUBSONIC FLOW

M. R. Soltani* and M. B. Bragg**
The Ohio State University
Columbus, Ohio

and

J. M. Brandon+
NASA Langley Research Center
Hampton, Virginia

ABSTRACT

A series of low-speed wind tunnel tests on a 70-degree sharp leading-edged delta wing at both static and dynamic conditions were performed to investigate the aerodynamic forces and moments. Forces and moments were obtained from a six component internal strain gauge balance. Static results compared well with the previous experimental findings. Large amplitude dynamic motion was produced by sinusoidally oscillating the model over a range of reduced frequencies. Substantial force and moment overshoots, a delay in dynamic stall, and hysteresis loops between the values of aerodynamic loads in upstroke and downstroke motion were observed, all of which were strong functions of the reduced frequency. The aerodynamic forces and moments were influenced by the Reynolds number. Asymmetrical vortex bursting produced by non-zero sideslip angle created a complex rolling moment variations with angle of attack.

NOMENCLATURE

C_L	Lift Coefficient
C_D	Drag Coefficient
C_l	Rolling Moment Coefficient
C_M	Pitching Moment Coefficient
C_N	Normal Force Coefficient
$C_{N,\alpha}$	Variation of Normal Force Coefficient with Angle of Attack (/deg)
$C_{L,\alpha}$	Variation of Lift Coefficient with Angle of Attack (/deg)
$C_{D,\alpha}$	Variation of Drag Coefficient with Angle of Attack (/deg)
$C_{M,\alpha}$	Variation of Pitching moment Coefficient with Angle of Attack (/deg)
$C_{l,\alpha}$	Variation of Rolling moment Coefficient with Angle of Attack (/deg)

C	Wing Root Chord (ft)
U_∞	Tunnel Speed (ft/sec)
K	Reduced Frequency $2\pi FC/U_\infty$
F	Frequency (Hz)
R_e	Reynolds Number Based on the Root Chord
α	Angle of Attack (deg)
β	Sideslip Angle (deg)
Λ	Wing Sweep

I. INTRODUCTION

Since the early use of aircraft in combat, a consistent demand for extending the flight boundaries and for greater maneuverability have played a major role in the design of fighter airplanes [1-4]. Increased maneuverability requires flight through the high angle of attack regime which has proven to be of great advantage in the dog fight arena[1]. As a result, current and future fighter aircraft design trends are in favor of abandoning angle of attack limitations in low-speed flight [4,5]. Poststall situations usually occur under dynamic conditions when the aircraft is pitched rapidly through the angle of attack for static stall, and well beyond.

A first step toward achieving the aforementioned goals was the use of highly swept, slender, sharp leading-edge delta wings. The lift producing mechanism of these wings is different than that of other wings, mainly due to the formation of a pair of strong vortices at moderate to high angles of attack on the wing suction side. Their sharp leading edge prevents the approaching flow from remaining attached to the surface, as it does in the vicinity of round edges. Thus separation occurs, and results in the loss of leading-edge suction, a phenomenon which contributes greatly to the lift of two-dimensional airfoils [6,7]. This, along with their inherent low aspect ratio, results in low lift to drag ratios at subsonic speed, thus producing poor performance in this flight regime. However their extensive sweep angle provides favorable drag characteristics at high speed making supersonic flight practical [1].

Numerous subsonic experimental/theoretical studies have shown that the flow field around delta wings in steady flight at moderate to high angles of attack is dominated by a pair of spiral leading edge vortices [7-23]. These vortices induce additional velocities on the suction side of the wing, producing additional lift which is referred to as 'vortex lift' [8-9,24-25]. Vortex lift grows nonlinearly with increased incidence, and depending on the leading-edge sweep angle, may account for a large portion of the lift. Static experimental

*Graduate Research Assistant, Department of Aeronautical and Astronautical Engineering, Member AIAA

**Associate Professor, Department of Aeronautical and Astronautical Engineering, Senior Member AIAA.

+Aerospace Engineer, Flight Dynamics Branch, Member AIAA.

results of references 8 and 9 show that for a 75 degree leading-edge sweep delta wing, vortex lift amounts to 50% of the total lift. These vortices are stable over a wide range of angle of attack, up to 30 degrees for a leading-edge sweep of 70 degrees, therefore, producing high lift at high incidence.

Considerable experimental/theoretical research has focused on understanding the vortex bursting phenomenon and its aerodynamic effects on high performance aircraft. These sudden changes of the structure of the vortex core have a strong influence on the aircraft stability. When the aircraft is yawed, these vortices will burst asymmetrically over the wing causing changes in the lateral-directional stability [14-15,26-27].

Previous results obtained from studies of three-dimensional oscillating models indicate a different flow structure over the upper surface of the wing between the up and downstroke motions [6,28-34]. It has been suggested [6,29] that increasing the oscillation-frequency will widen the hysteresis loop, a phenomenon caused by the lag in flow separation and reattachment due to the fast variation of the angle of attack. Studies which attempt to predict or experimentally measure the aerodynamic advantages or disadvantages associated with dynamic flow over three-dimensional lifting surfaces have not been extensive. Due to current emphasis on supermaneuverability at high incidence for the future generation of high performance aircraft, an understanding of the dynamic aerodynamic effects are essential.

A series of low-speed wind tunnel tests on a 70 degree sharp leading-edge delta wing model with and without a fuselage were conducted. These investigations were performed to find the effect of large amplitude dynamic motion on longitudinal and lateral forces and moments. Tests included oscillating the delta wing model in pitch at several sideslip angles to explore the effect of asymmetric vortex bursting on model forces and moments.

II. EXPERIMENTAL PROCEDURE

The experiments were conducted in the subsonic wind tunnel of The Ohio State University located at the Aeronautical and Astronautical Research Laboratory (OSU/AARL). The tunnel test section is approximately five feet wide, three feet high, and eight feet long, and operates at speeds from 0 to 220 ft/sec at Reynolds number of up to $1.3 \cdot 10^6$ per foot. The tunnel is of open return type and uses four large anti-turbulence screens and honeycomb to attain a low turbulent intensity through the test section [35].

Models

Two different models were used to perform these experiments. One which resembles a generic fighter model, consists of a very simple cylindrical fuselage on which a number of different forebodies can be mounted. The fuselage has a diameter just large enough to accommodate the six component internal strain gauge balance and the necessary attachment hardware. The fuselage is combined with a 70-degree sharp leading-edge delta wing with a one-foot span, a tail cone, and a sharp wooden circular cross section nose with a fineness ratio (l/d) of 1.5. A fiberglass skin was used over a carbon fiber reinforced foam core. A sketch of this model is shown in figure 1.

The second model was a simple flat plate delta wing of 70 degree leading-edge sweep, a 20.61 inch root chord and a 15 inch span at the trailing edge. The wing was constructed of 1/2 inch thick plywood (.024 thickness to chord ratio) and had sharp beveled leading and trailing edges. A pod large enough to house the balance and necessary hardware was attached under the wing. A drawing of the model used in this investigation is shown in figure 2.

Oscillation System

A system was designed to pitch the models through large amplitude oscillations. This apparatus is shown in figure 3. The oscillation system uses a belt and pulley arrangement to obtain oscillation frequencies of 0 to 2.3 hertz. The last pulley in the system drives a cam which produces a sinusoidal pitching motion of the model from 0 to 55 degrees angle of attack. The present system also allows sinusoidal pitching motion at steady sideslip angles to +15 degrees in increments of 5 degrees. A potentiometer mounted on the arm of the oscillation system provides the instantaneous angle of attack of the model. The delta wing model was pitched about the 57 percent root chord location while the pitch axes for the generic fighter was at the 39 percent root chord location. The Z-location of the pitch axis was about 3.12 inches below the wing chord line for both models. Figure 4 shows the measured sinusoidal variation of angle of attack with time at different frequencies.

Velocity Measurement

A hot-wire probe was used in conjunction with the pressure transducers to accurately determine the freestream velocity variations during static and pitching oscillation. The hot wire probe was placed in the center of the tunnel test section and at one chord length upstream of the model. The results from the hot wire data and those of the pressure transducers were in excellent agreement for all the reduced frequencies tested.

Force Measurement

Force measurements were made using a six-component internal strain gauge balance on loan from NASA Langley Research Center. The balance was statically calibrated at the OSU/AARL. The calibration results are in good agreement with earlier calibration of the balance provided by NASA Langley.

Tare Measurement

There are two types of forces and moments acting on the balance when the model is oscillating in the wind tunnel for the wind-off tests. The first are the gravitational loads due to the model and balance weight which are functions of the angle of attack. The second are the inertial forces and moments produced by the moments of inertia of the oscillating model and balance. Both of these forces and moments must be measured and subtracted from the wind-on data [42].

The magnitude of model, wind-off loads were calculated in a straightforward manner based on geometry and oscillation frequency. From experimental measurements it was found that the internal strain gauge balance itself made a considerable contribution to these tares. After removing the balance alone tares from those of the balance with model installed, the calculated tares compared very well with the measured ones. These comparisons indicated that the effect of the surrounding still air on the model as it oscillates,

wind off, is negligible. These tares were fit for each case as a function of angle of attack using a polynomial and later were subtracted from the measured loads.

Data Acquisition And Reduction

The data acquisition system used in this investigation was developed at the OSU/AARL. Data were taken and reduced on an IBM PC/AT. The IBM is equipped with a 12 bit 16 channel Analog to Digital board capable of a sample rate of 27.5 KHz. For this experiment 10 channels of data were measured: 6 for balance data, 1 for potentiometer input, 2 for tunnel speed, and 1 hot film channel. Figure 5 shows the complete set-up for these experimental studies.

Dynamic data presented in this paper are an average of several cycles at a sample rate based on the reduced frequencies. Data were taken and reduced on the IBM PC/AT and uploaded to the main laboratory computer. The data were then digital filtered and plotted as a function of time and or angle of attack. Figure 6 compares the digital and analog filtered normal force data with the unfiltered case. The digital filtered data more accurately represent the measured forces and are used to present the data in this report.

Aerodynamic forces and moments were measured at the balance moment center and have been transferred to the 25% wing root chord station. All moments were nondimensionalized with respect to 2/3 wing root chord. Longitudinal forces and moments are in the wind axis system and lateral-directional forces and moments are in the body axis system [36].

Blockage corrections at small angle of attack were determined by the method of reference 36 and were found to be small. In addition reference 38 suggests that blockage ratios of less than 7% can usually be considered negligible. The blockage ratio for this investigation was 6%. Thus no correction has been applied to the data.

III. RESULTS AND DISCUSSION

The purpose of this experimental investigation was to study the effect of large amplitude motions, at high angles of attack, on the aerodynamic characteristics of three dimensional lifting surfaces. In these experiments the aerodynamic forces and moments of a 70 degree sharp leading-edge delta wing, undergoing simple sinusoidal motion at various Reynolds numbers and reduced frequencies, were measured using a six-component internal strain gauge balance. Both models were first tested under static conditions to compare with other wind tunnel results. Delta wing model static data are examined first, followed by the dynamic results.

Static Tests

The variation of longitudinal forces and moments of the delta wing model with angle of attack, at zero sideslip angle and at several Reynolds numbers are examined first. The effect of sideslip variations on the aerodynamic characteristics of the model at a constant Reynolds number are then studied and are compared with the zero sideslip data. The present zero sideslip results are compared, where possible, with the previous findings of [8,10] and the theoretical data of [24]. The data for each angle are an average of several hundred samples over a period of 10-15 seconds.

Reynolds number effect: The static variation of normal force coefficient with angle of attack for the chord Reynolds numbers of $1 \cdot 10^6$ to $1.97 \cdot 10^6$ is shown in figure 7. The nonlinear variation of normal force with increasing angle of attack for all the Reynolds numbers tested is clear. From figure 7, it is evident that increasing Reynolds numbers will decrease the maximum normal force. It has been suggested that increasing the Reynolds number will move the boundary layer transition forward [17,20], thus causing the reduction in normal force.

Figure 8 shows the static variation of the lift coefficient with angle of attack at the aforementioned root chord Reynolds numbers. Again the nonlinearity in lift with the angle of attack is quite clear. This nonlinearity is a result of the coupling of the potential flow at low angle of attack with the vortex lift generated by the delta wing geometry at moderate to high incidence. This phenomenon is clear from figure 8 when the experimental data are compared with the predicted values of lift coefficient using the potential flow and the method of reference 24. Note that for small incidence, the experimental data compare well with the predicted potential flow lift. It should be noted that at zero angle of attack, the lift coefficient for the present experiment has a small negative value which is probably caused by the presence of the pod (balance cover) under the model.

As the angle of attack increases, the experimental data deviates from that predicted by the potential theory. Deviation of the measured data from the potential theory indicates that additional lift is generated by the delta wing model. This additional lift is produced due to the development of a pair of vortices emanating from the wing leading edge proceeding downstream. These vortices are called 'fully developed' [25] when they reach the wing trailing edge. In reference 24, a method for calculating this vortex lift for a no camber, no twist, thin, and sharp leading-edge wing has been developed. The predicted results for the present model are plotted on figure 8. The experimental results are in good agreement with Polhamus' theory of reference 24. The discrepancy is probably due to the small leading edge radius of the present model and the balance pod. Large deviation between the experimental and theoretical values above an incidence of 28 degrees are caused by the bursting phenomenon which was not considered in the theory of reference 24. Good agreement was achieved when the present results were compared with the experimental data by Wents [9] and Hummel [10].

Figure 9 shows the effect of Reynolds number on drag coefficient. The present results are in excellent agreement when compared with the experimental results of reference 10. From figure 9 it appears that drag is less dependent on Reynolds number than is lift. However, increasing the Reynolds number will cause a slight decrease in drag which is due to the corresponding reduction of lift.

Figure 10 shows the static longitudinal pitching moment development with increasing angle of attack at various Reynolds numbers. At zero angle of attack, the presence of the slight (nose up) pitching moment shown in figure 10 is probably the result of the negative normal force, shown in figure 7 and 8, produced by the balance pod. By

increasing the angle of attack, the delta wing produces a negative pitching moment which indicates that the center of pressure moves aft of the referenced point (1/4 wing root chord). For angles less than the critical angle, the angle of attack at which the vortex burst point crosses the trailing edge, $C_{m,\alpha}$ has an almost constant negative value. However, when the angle of attack is significantly larger than the critical value, $C_{m,\alpha}$ becomes positive, due to a reduction in the nose down pitching moment. As the vortex burst point progresses forward, $C_{m,\alpha}$ changes sign due to the loss of lift on the rear portion of the wing [10,11]. Increasing the Reynolds number also reduces the nose down pitching moment, but the slope of $C_{m,\alpha}$ does not change significantly.

Sideslip effect: The effect of asymmetrical vortex bursting on the static lateral and longitudinal forces and moments characteristics were investigated by variation of the sideslip angle from 0 to +15 degrees in increments of 5 degrees. The model was set to the desired sideslip and the angle of attack was varied from 0 to 55 degrees. All runs were made at a root chord Reynolds number of 1.64 million.

Figure 11 shows the resulting normal force coefficient at sideslip angles of 5, 10, and 15 degrees, versus angle of attack. Also for comparison, the data for zero sideslip angle are presented. An obvious effect of sideslip angle is the reduction of normal force. However, increasing the sideslip angle also shifts the maximum normal force to a higher angle of attack, and produces an abrupt stall due to an increase in the effective sweep of the leeward wing. As a result of the sideslip angle, asymmetrical vortex bursting occurs over the wing surface. This phenomena is clear for the sideslip angles of 10 and 15 degrees of shown in figure 11. Here the variation of $C_{N,\alpha}$ with alpha has a local minima, when the windward vortex burst point reaches the trailing edge of the wing, before the stall angle is reached. For the other longitudinal forces and moments the effect of sideslip angle variation is similar.

Figure 12 shows static variation of the rolling moment coefficient with angle of attack at several sideslip angles. It is evident that at zero sideslip, the rolling moment coefficient is not zero. This slight variation is possibly due to slight asymmetry in the model, or perhaps a small sideslip angle caused by misalignment of the model in the airstream. At non-zero sideslip angle the effective sweep in the windward wing decreases ($A = 70-\beta$) while the sweep of the leeward wing increases ($A = 70+\beta$). As a result, the vortex burst point crosses the windward wing trailing edge at a lower incidence than it does for the leeward wing, asymmetrical vortex bursting.

Figure 12 shows a negative rolling moment initially at 15 degrees sideslip. The absolute value of the rolling moment coefficient increases up to an incidence of about 17-18 degrees. This angle of attack coincides with the C_N data which indicate that bursting had reached the windward wing trailing edge. Further increase of the incidence is followed by the reduction in absolute value of the rolling moment until the bursting reaches the windward wing apex which creates an inflexion region in the normal force ($\alpha = 25-29$

deg). This inflexion region is evident by examining the variation of the gradient of the rolling moment with angle of attack, $C_{l,\alpha}$, where the gradient drops markedly. At an incidence of about 34 degrees, the rolling moment reverses again. Interestingly enough, this once more agrees with the reduction of the gradient of the normal force. This time the change in the rolling moment corresponds to the vortex burst point crossing the leeward wing trailing-edge. The rolling moment reaches a second local maximum absolute value at an incidence of about 43-45 degrees where $C_{N,\alpha}$ changes sign as a result of the loss of lift caused by the vortex burst point reaching the leeward wing apex. The vortex inception angles for both leeward and windward wing compares well with the results of references 8 and 26.

Dynamic Tests

Dynamic tests were performed by sinusoidally oscillating the model from 0 to 55 and back to zero degrees angle of attack. Data for each cycle are taken at a frequency of 100-1000 Hz and up to 1000 data points are collected.

Substantial maximum force and moment overshoots, delay in stall angle of attack, and large hysteresis between increasing and decreasing angle of attack are seen for even the smallest frequency tested, .2 Hz. During the upward motion, the vortex burst point crosses the trailing edge at a higher angle of attack than it does in the static case, which results in higher forces and moments, and then, during downward motion, the flow remains separated until angles of attack below static stall, creating a hysteresis loop. Comparisons with the static forces and moments show that during downstroke motion, the static values are higher than the dynamic values for all the reduced frequencies tested. Variation of the pitch rate had a great influence on the flow characteristics over the model. As a result of these changes in the flow structure, the deviation between the dynamic and static forces and moments vary, and so do the width of the hysteresis loops.

In the experiment reported herein, the aerodynamic forces and moments of the 70-degree sharp leading-edge delta wing at various Reynolds numbers, reduced frequencies, and sideslip angles are presented. Comparisons between static and dynamic results, where applicable, are made. Finally, variation of the static and dynamic normal force of both models with angle of attack are compared.

Reynolds number effect: Dynamic variation of normal force with angle of attack for Reynolds numbers of 1×10^6 to 1.97×10^6 and a reduced frequency of .074 is shown in figure 13. Reduced frequency was kept constant by varying the oscillation frequency with tunnel speed. Also, as a comparison static values for a Reynolds number of 1×10^6 are shown on the plot. As in the static case, increasing Reynolds number seems to promote the vortex bursting which results in the reduction of the normal force. The angle of attack at which the reduction of the gradient, $C_{N,\alpha}$, begins, is an indication of the vortex burst point crossing the trailing edge. The vortex burst point reaches the trailing edge at smaller angles of attack as Reynolds number is increased. This bursting will decrease the upper surface suction considerably, and as a result the

slope of the the normal force curve will drop markedly as the angle of attack is increased further. Also, from figure 13, it is clear that the dynamic data for Reynolds number of 1×10^6 shows a substantial maximum normal force overshoot, and delay in stall angle of attack when compared with the static data of the same Reynolds number. For other Reynolds numbers the trend between dynamic and static normal force are the same. The relationship of these changes between dynamic and static data along with the large hysteresis loop between upward and downward motion will be discussed in a later section.

Figure 14 shows the dynamic variation of the lift coefficient with angle of attack for the aforementioned Reynolds numbers and is compared with the static data for a Reynolds number of 1×10^6 . Again the effect of Reynolds number is clearly evident. Substantial increase in lift coefficient for dynamic case is observed when compared to the static case at the same Reynolds number. Comparison of the static and dynamic lift coefficient for other Reynolds numbers show the same trend.

The drag performance of the three dimensional delta wing undergoing sinusoidal pitch oscillation at various Reynolds numbers and constant reduced frequency is compared with the static case at a Reynolds number of 1×10^6 in figure 15. The increase in drag force at high α for the dynamic case is evident in comparison with the static case. This is not surprising since the dynamic normal force shows the same trend. The same results are obtained when comparing the static and dynamic drag forces for other Reynolds numbers. There is some decrease in drag for increasing Reynolds number which is most probably due to the reduction in the lift (fig. 14). Also, the angle of attack at which the maximum value of the drag is found is independent of the Reynolds number.

Figure 16 shows the development of the pitching moment coefficient with angle of attack for the three Reynolds numbers mentioned and at a fixed reduced frequency. Again, as a comparison, the static data of Reynolds number of 1×10^6 is presented. The dependency of the pitching moment on Reynolds number variations is evident. Higher Reynolds number promotes bursting, which will alter the variation of the $C_{m,\alpha}$ with angle of attack. Ultimately, at higher incidence, $C_{m,\alpha}$ will change sign. From figure 16 it is clear that as the Reynolds number increases, the onset of deviation of $C_{m,\alpha}$ with the angle of attack occurs at a lower incidence. This observation coincides with those of the normal force, explained previously. The reduction in normal force due to the forward progression of the vortex burst point on the wing lessens the nose down pitching moment.

Effect of reduced frequency: As mentioned previously, reduced frequency has a substantial influence on the complicated three dimensional flow over the oscillating model. In order to thoroughly investigate these effects, the sharp leading-edge delta wing model was sinusoidally oscillated in pitch at various reduced frequencies ($k = .015-.405$). In the following sections the results for a root chord Reynolds number of 1.64×10^6 and reduced frequencies of $k = .03$ to $.165$ will be presented.

Figure 17 presents the normal force coefficient versus angle of attack for the previously mentioned reduced frequencies. Static data are also plotted as a baseline. For $k = .03$, the value of $C_{N,\alpha}$ starts to decrease at an angle of about 30 degrees, while for the static case, this occurs at an angle of about 23 degrees. This is an indication of the delay in separation and vortex bursting during the dynamic upward motion. When the vortex burst point crosses the trailing edge, further increase in the incidence results in the vortex burst point moving onto the wing, thus reducing vortex lift contribution to the normal force. As the reduced frequency is increased, the flow lag effect increases and results in the higher maximum C_N values (fig. 17).

In the downstroke motion, the flow starts reattaching from the wing apex and progresses toward the trailing edge. During the downward motion for the $k = .03$ data, the variation of $C_{N,\alpha}$ with α drops from a large positive value to its maximum negative value at an angle of about 42 degrees. This probably indicates that the flow remains separated until an angle of 42 degrees in downward motion. From here on, the leading edge vortices start attaching to the suction side from the wing leading edge and proceeds back to the trailing edge. At an angle of about 23-25 degrees $C_{N,\alpha}$ reaches the same value as it had in the upstroke motion. These differences in $C_{N,\alpha}$ between upstroke and downstroke motion are caused by the flow lag effect which creates the hysteresis loop. At higher reduced frequency, the effect of the flow lag is more pronounced and produces a wider hysteresis loop (fig. 17).

The dynamic variation of the lift coefficient with angle of attack for various reduced frequencies is shown in figure 18. Comparison of the dynamic data with the static case at the same Reynolds number clearly shows increase in maximum lift and delayed separation for all cases reported. Increasing the pitch rate has a significant influence on the dynamic stall angle. Maximum lift overshoot did not vary significantly with reduced frequency in contrast to the normal force data. This is probably due to the increase in axial force at higher reduced frequency.

Figure 19 shows the effect of reduced frequency on drag coefficient during large amplitude sinusoidal motions. A much higher drag is evident at high angle of attack for the pitch-up motion compared with the static case. While on the downstroke motion, the hysteresis in the dynamic drag curve shows substantial reduction in drag when compared to the static data. These variations in drag during up and down motions are probably due to the variations of the normal force discussed previously. The influence of pitch rate on the character of drag force hysteresis loop and its magnitude is apparent.

Dynamic variation of drag due to lift at various reduced frequencies is shown in figure 20. As explained earlier, note that increasing the reduced frequency will slightly increase the maximum lift overshoot, and more drag is produced. However, the increase in drag is more pronounced.

Figure 21 shows the corresponding pitching moment data of the model for both the static and

dynamic cases. Again, the influence of reduced frequency on the pitching moment hysteresis loop and its magnitude is apparent. As the burst point crosses the trailing edge, the onset of deviation of normal force with alpha reduces the magnitude of $C_{m,\alpha}$. Ultimately increasing the incidence results in the loss of lift, and a change in the sign of $C_{m,\alpha}$. During pitch up motion a much larger negative pitching moment is evident compared to the static value due to delay of vortex bursting, while on the downward motion the dynamic pitching moment has a substantially smaller negative value due to delay reattachment.

Sideslip effect: As in the static case, the effect of sideslip variation on the aerodynamic forces and moments of the model were investigated by manually setting the model to the desired sideslip angle (+15 degrees in increment of 5 degrees). The model was then oscillated sinusoidally at various reduced frequencies. In the following sections, longitudinal and lateral force and moment data at sideslip angles of 0 to 15 degrees and at a constant reduced frequency will be examined first. Due to the symmetry in the data, negative values for the sideslip will not be discussed. However, to show the symmetry in the results, the values of the rolling moment coefficient for -15 degrees sideslip will be presented. The effect of reduced frequency on the model forces and moments with non-zero sideslip angle will be considered later. The following data are all at a constant root chord Reynolds number of 1.64×10^6 .

Dynamic lift and normal force coefficient curves at sideslip angles of 0, 5, 10, and 15 degrees and $k=.043$ are shown in figures 22 and 23. As in the static case, the immediate effect of sideslip at moderate to high alpha is a substantial reduction in the normal force. From figure 23, note that the onset of deviation of $C_{N,\alpha}$ with angle of attack for a sideslip of 15 degrees occurs at an angle of about 19 degrees, while for the static case this happened at an incidence of 17 degrees, a result of the reduced frequency. By further increasing the incidence, the vortex burst point on the windward wing, with 55 degree sweep, will move upstream, at an angle of about 35 degrees $C_{N,\alpha}$ has a local minima as shown in figure 23. This indicates that the windward vortex burst point has reached the apex of the wing. However, as the angle of attack is increased further, the leeward vortex burst point crosses the trailing edge, reducing $C_{N,\alpha}$ once again. From figure 23, note that as the sideslip angle increases, dynamic stall occurs at a higher angle, a phenomenon also observed in the static case.

Figures 24 and 25 show the dynamic variation of the drag force and pitching moment of the 70-degree sharp leading-edge delta wing at the reduced frequency of $K=.043$ and the aforementioned sideslip angles. Increasing sideslip angle reduces both drag and pitching moment. The angle at which $C_{N,\alpha}$ has a local minimum before reaching the stall incidence is clearly seen from both figures for sideslip angles of 10 and 15 degrees. This discontinuity is caused by the asymmetrical vortex bursting on the wing at non-zero sideslip angles.

The complex variation of the rolling moment coefficient with angle of attack at various

sideslip angles, and for a constant reduced frequency of $K=.043$, is shown in figure 26. Hysteresis loops in the rolling moment coefficient during upward and downward motion are evident. The dramatic behavior of the rolling moment with angle of attack for all sideslip angles tested is caused by asymmetrical vortex bursting on the wing. In upward motion, note that the rolling moment curve has two minima for all sideslip angles. The first minima is the result of the vortex burst point crossing the windward trailing edge, due to its effective sweep reduction. The local maximum, after the first minimum, marks the angle of attack where the leeward wing vortex burst point reaches the trailing edge of the wing. The second minima corresponds to the leeward vortex burst point reaching the vicinity of the wing apex. Except for the magnitude and the location of the maxima and minima in the variation of the rolling moment with angle of attack, the upstroke variations of the rolling moment for this low reduced frequency correlates with the static case discussed previously. For the static case, experimental results of reference [9] for an 85 degree sweep delta wing shows vortex bursting crossing the trailing edge at an incidence of about 37 degrees. Here, the vortex burst point crosses the leeward wing trailing edge at an incidence of about 38 degrees, a good comparison.

Dynamic variation of rolling moment coefficient with the angle of attack in downstroke motion is somewhat different than the upward motion. From figure 26, for 15 degree sideslip angle case, note that the rolling moment coefficient is almost constant for incidences of 55 to about 43 degrees during the downstroke motion. This phenomena was seen at all sideslip angles. This is probably due to the fact that the separated vortices created in upstroke motion remain separated, even as alpha is decreased, due to the rapid change of the incidence [6,17]. Hence the flow over the wing lags these rapid changes. From angles of about 33 to 28 degrees the rolling moment increases due to the formation of the leeward wing vortices from the wing apex. As the windward vortex forms on the wing apex, the rolling moment coefficient reverses once again and its value decreases with the reduction of the angle of attack. At an incidence of about 16 degrees, the rolling moment coefficient in downward motion has the same value as it did in the upward motion, thus closing the hysteresis loop. Dynamic asymmetrical vortex bursting for -15 degrees sideslip clearly shows the same effect and is almost symmetric with the sideslip angle of 15 degrees.

Figures 27 and 28 show the variation of the normal force and lift coefficient with angle of attack at 15 degrees sideslip angle and reduced frequencies ranging from $K=.03$ to $K=.165$ and are compared with the static data at the same sideslip angle. Substantial increases in the maximum forces due to the oscillation are evident and are a strong function of the reduced frequency. However, in contrast to the zero sideslip case the maximum value of the lift coefficient is seen here to be a stronger function of the reduced frequency. For all the reduced frequencies reported, the local minima in the slope of $C_{N,\alpha}$ and $C_{L,\alpha}$ versus alpha occur at higher angle of attack as the reduced frequency is increased. As mentioned previously, this local minima in the slope indicates that the windward vortex burst point has reached the wing apex. Delay in dynamic stall with increasing

reduced frequency is evident from figure 28.

Figure 29 shows the effect of reduced frequency on rolling moment coefficient at 15 degrees sideslip angle. The complex behavior of the dynamic rolling moment was due to flow lags, as discussed previously. The magnitude of the rolling moment in upward motion increases with the increase in pitch rate, while in downstroke motion, the trend is different. Again, as the reduced frequency increases, the hysteresis loop widens. Also, in downstroke motion from the maximum incidence, the variation of the rolling moment coefficient with angle of attack remains constant for a wider range of angles of attack as the reduced frequency increases. This is clear in figure 29 for a reduced frequency of .165 in which the rolling moment coefficient is almost constant from incidence of about 48 degrees to about 22 degrees which indicates that the effect of flow lag has become more pronounced.

Effect of Fuselage

Up to this point all the data presented has been for the delta wing alone model. Comparison of the normal force performance of both the delta wing and delta wing with fuselage models for static and dynamic cases are shown in figure 30. It is evident that delta wing alone produces more normal force for both the static and dynamic cases. However, it appears that dynamic stall remains at almost the same angle of attack for both models. Dynamic results show that for the same reduced frequency, the width of the hysteresis loop for both models differs. At a reduced frequency of .068, the delta wing has a wider hysteresis loop than the delta wing with fuselage.

ACKNOWLEDGEMENT

This work was supported in part by a grant from NASA Langley Research Center. The authors would like to thank Mark Ringer and Jim Negro, Undergraduate Research Assistants, for their help in acquiring and reducing the data for this report.

IV. SUMMARY AND CONCLUSION

An extensive experimental program was conducted at the OSU/AARL to investigate the complex flow mechanisms on a delta wing undergoing large amplitude pitching oscillation. Two models were used to perform the experiments. Aerodynamic forces and moments at both static and dynamic conditions, and at various Reynolds numbers, were measured using a six component internal strain gauge balance. Also, to investigate asymmetrical vortex bursting and its effects on the aerodynamic loads, tests with sideslip angles of 0 to +15 degrees were conducted. Pitching motion was produced by sinusoidally oscillating the model between 0 and 55 degrees angle of attack at various reduced frequencies. Good results were obtained when the present static data were compared with previous findings. Also, the data compares well to Polhamus' leading edge suction analogy for predicting the lift coefficient at incidence below the critical angle.

The following observations summarize the results of this experimental program:

1) Dynamic forces and moments show a significant overshoot at all the reduced frequencies examined when compared to the static data and are strong functions of the pitch rate. Static stall occurs at a smaller angle of attack

than the dynamic one, which is a result of flow lags in the vortex burst progression over the suction side of the model.

2) Even at the lowest frequency tested, $F=2$ Hz, a hysteresis loop between increasing and decreasing angle of attack is observed in the force data. Increasing the pitch rate resulted in larger forces and moments in the upstroke motion. However, in downward motion, the flow remains separated until angles well below stall, hence the hysteresis loop widens.

3) Both dynamic and static data show a change due to the Reynolds number variations. As reported by other researchers, increasing Reynolds number will enhance the vortex inception angle, thus resulting in lower values of the forces and moments. These effects were clearly detected in the experimental data.

4) Non-zero sideslip angle resulted in asymmetrical vortex bursting over the model which was obvious from the variation of the rolling moment coefficient with angle of attack. At all non-zero sideslip angles tested, a remarkable drop in all of the aerodynamic forces and moments at both static and dynamic conditions were observed. The rolling moment curve varied in a complex way with the angle of attack at non-zero sideslip angles. This variation along with those of other forces and moments compared well with the previous data obtained by other researchers for the static case. Variation of sideslip angle also verifies the fact that wing sweep angle has a substantial influence on the vortex inception angle.

5) Variations of rolling moment with angle of attack at all sideslip angles tested, is again, a strong function of the reduced frequency. Absolute values of the rolling moment increase with increasing pitch rate. For $K=.165$, it was clearly seen that in downstroke motion, rolling moment remained almost constant for a wide range of incidence, indicating the flow remained separated below static stall angle of attack.

Although the present work was performed on a simple delta wing model using a simple sinusoidal oscillation, the results obtained show significant differences between the dynamic and static aerodynamic characteristics which will have strong influence on a high performance aircraft's maneuverability. Thus far, the experimental method has been established, and now a more thorough investigation of the character of the dynamic, complex, three-dimensional flow field over different models with different wing geometries under various motion is possible. Future tests will examine detailed flow visualization results. Also, aerodynamic forces and moments at a more realistic flight profile will be studied. These investigations along with those of other researchers hopefully will provide a detailed understanding of the flow structure and its influence on the aerodynamic properties of supermaneuverable aircraft.

REFERENCES

1. Polhamus, Edward C.: Vortex Lift Research: Early Contributions and Some Current Challenges. NASA Conference Publication 2416, Volume I, 1986.
2. Polhamus, E. C.: Applying Slender Wing Benefits to Military A/C. Journal of Aircraft, Vol. 21, No. 8, August 1984.

3. Nelson, R. C.: The Role of Flow Visualization in the Study of High Angle of Attack Aerodynamics. Tactical Missile Aerodynamics edited by Hensch, M.J. and Nielson, J.N., 1986.
4. John, H. and Kraus, W.: High Angle of Attack Characteristics of Different Fighter Configurations. AGARD-CP-244, 1978, pp. 2-1 to 2-15.
5. Brandon, Jay M., and Nguyen, Ho, T.: Experimental Study of Effects of Fore-body Geometry on High Angle of Attack Static and Dynamic Stability. AIAA Paper No. 86-0331, Nov. 1985.
6. Gad-el-Hak, Mohamed, and Ho, Chih-Ming: The Pitching Delta Wing. AIAA Journal, Vol. 23, No. 11, Nov. 1985.
7. McCormick, B. W.: Aerodynamics, Astronautics, and Flight Mechanics. John Wiley and Sons, 1979, pp.294-302
8. Wentz, William H.: Wind Tunnel Investigations of Vortex Breakdown on Slender Sharp-Edged Wings. PHD Dissertation, University of Kansas, 1968.
9. Wentz, W. H., and Kohlman, D. L.: Vortex Breakdown on Slender Sharp Edged Delta Wings. AIAA Paper No. 69-778, July 1969.
10. Hummel, D., and Srinivasan, P. S.: Vortex Breakdown Effects on the Low-Speed Aerodynamic Characteristics of Slender Delta Wings in Symmetrical Flow. Journal of the Royal Aeronautical Society, April 1967.
11. Hummel D.: On the Vortex Formation Over a Slender Wing at Large Angles of Incidence. AGARD-CP-247, 1978, pp.15-1 to 15-17.
12. Payne, Francis M.: The Structure of Leading Edge Vortex Flows Including Vortex Breakdowns. PHD Dissertation, University of Notre Dame, 1987.
13. McKernan, J. F., and Nelson, R. C.: An Investigation of the Breakdown of the Leading Edge Vortices on a Delta Wing at High Angles of Attack. AIAA Paper No. 83-2114, August, 1983.
14. Hall, Robert M.: Influence of fore-body Cross Sectional Shapes on Wing Vortex-Burst Locations. Journal of Aircraft, Vol. 24, No. 9, Sept. 1987.
15. Boyden, Richard P.: Effect of Leading-Edge Vortex Flow on the Roll Damping of Slender Wings. Journal of Aircraft, Vol. 8, No. 7, July 1971.
16. Payne, F. M., and Nelson, R. C.: Experimental Study of the Velocity Field on a Delta Wing. AIAA Paper No. 88-0122, January 1988.
17. Schrader, Karl F., Reynolds, G. A., and Novak, C.J.: Effect of Mach Number and Reynolds Number on Leading-Edge Vortices at High Angles of Attack. AIAA Paper No. 88-0122, January 1988.
18. McCune, J. E., Tavaras, T. S., Lee, K. W., and Weissbein, D.: Slender Wing Theory Including Regions of Embedded Total Pressure Loss. AIAA Paper No. 88-0320, January 1988.
19. Shi, Z., Wu, J. M., and Vukili, A. D.: An Investigation of Leading Edge Vortices on Delta Wings With Jet Blowing. AIAA Paper No. 87-0330, January 1987.
20. Kjelguard, Scott D., Sellers III, William, L., and Watson, Robert, P.: The Flowfield Over a 75 Degree Swept Delta Wing at 20.5 Degrees Angle of Attack. AIAA-86-1775, June 1986.
21. Jun, Y. W., and Nelson, R. C.: Leading Edge Vortex Dynamics on a Delta Wing Undergoing a Wing Rock Motion. AIAA Paper No. 87-03320 January 1987.
22. Hoeijmakers, H. W. M., and Bennekens, B.: A Computational Model for the Calculation of the Flow About Wings With Leading Edge Vortices. AGARD-CP-247. pp. 25-1 to 25-11.
23. Elle, B. J., and Jones, J. P.: A Note on the Vorticity Distribution on the Surface of Slender Delta Wing with Leading Edge Separation. Journal of the Royal Aeronautical Society, March 1961.
24. Polhamus, E. C.: Prediction of Vortex-Lift Characteristics by Leading-Edge Suction Analogy. Journal of Aircraft, Vol. 8, No. 4, April 1971.
25. Hoerner, Sigward F., and Brost, H. V.: Fluid Dynamic Lift. Hoerner Fluid Dynamics, 1975, pp. 18-1 to 18-20.
26. Skow, A. M., Tiriga, J. R., and Moore, W. A.: Forebody/Wing Vortex Interactions and Their Influence on Performance and Spin Resistance. AGARD-CP-247, No.6, pp. 6-1 to 6-26.
27. Genxing, Wu, Tzehsing, Wang, and Shixhong, Tian: Investigation of Vortex Patterns on Slender Bodies at High Angles of Attack. Journal of Aircraft, Vol.23, No. 4, April 1986.
28. Nguyen, Luat, T., Whipple, Raymond D., and Brandon, Jay M.: Recent Experiments of Unsteady Aerodynamic Effects on Aircraft Flight Dynamics At High Angles of Attack. AGARD-CP-386, 1985 pp. 28-1 to 28-30.
29. Gad-el-Hak, Mohamed, and Ho, Chih-Ming. Unsteady Vortical Flow Around Three Dimensional Lifting Surfaces. AIAA Journal, Vol. 24, No. 5, May 1986.
30. Robinson, M. C., and Wissler, J. B.: Unsteady Surface Pressure Measurements on a Pitching Rectangular Wing. AIAA Paper No-88-0328, January 1988.
31. Gilliam, F., Wissler, J., Robinson, M., and Walker, J.: Visualization of Unsteady Separated Flow About a Pitching Delta Wing . AIAA Paper No-87-0240.

32. Ashworth, J., Mouch, T., and Luttgies, M.: Application of Forced Unsteady Aerodynamics to a Forward Swept Wing X-29 Model. AIAA Paper No-88-0563, January 1988.
33. Levin, D., and Katz, J.: A Vortex-Lattice Method for the Calculation of the Non-Steady Separated Flow over Delta Wings. AIAA Paper No-88-0563, January, 1980.
34. Wolffelt, Karl W.: Investigation of the Movements of Vortex Burst Position with Dynamically Changing Angle of Attack for a Schematic Delta Wing in a Water Tunnel With Correlation to Similar Studies in a Wind Tunnel. AGARD.
35. Soltani, M. R.: Experimental Studies of the Effect of Ice Formation on the Aerodynamics of an Axisymmetric Body. M. S. Thesis, The Ohio State University, 1986.
36. Rae, W. H., and Pope, A.: Low-Speed Wind Tunnel Testing. Second Edition, John Wiley and Sons, 1984.
37. Malcolm, G. M., and Schiff, L. B.: Recent Developments in Rotary-Balance Testing of Fighter Aircraft Configurations at NASA Ames Research Center. AGARD-CP-386, 1985, pp. 18-1 to 18-25.
38. Pass, C. Q.: A Wake Blockage Correction Method for Small Subsonic Wind-Tunnels. AIAA Paper No. 87-0294, January 1987.

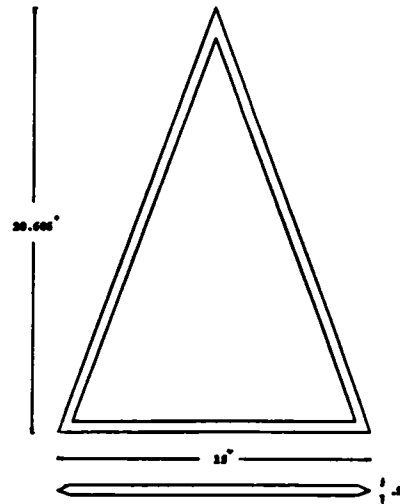


FIGURE 2. THE DELTA WING MODEL.

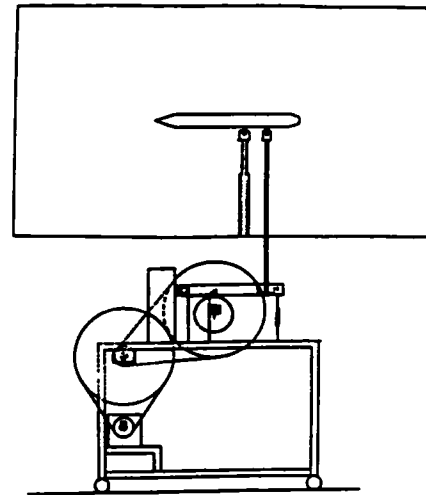


FIGURE 3. MODEL OSCILLATION SYSTEM.

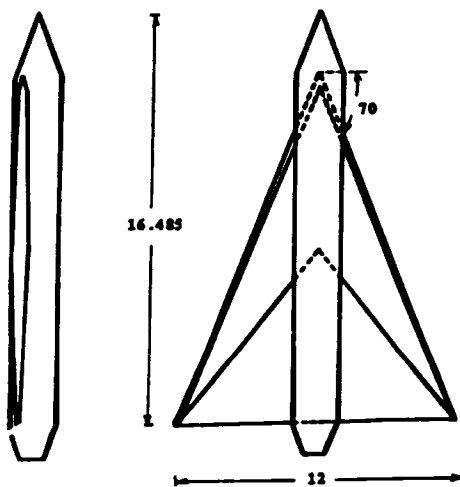


FIGURE 1. DELTA WING WITH FUSELAGE MODEL.

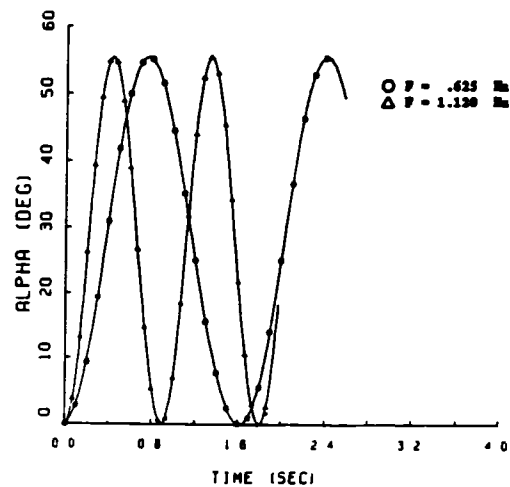


FIGURE 4. MEASURED VARIATION OF THE ANGLE OF ATTACK WITH TIME.

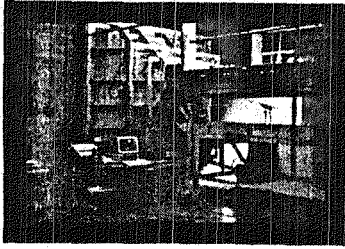


FIGURE 5. EXPERIMENTAL SET-UP.

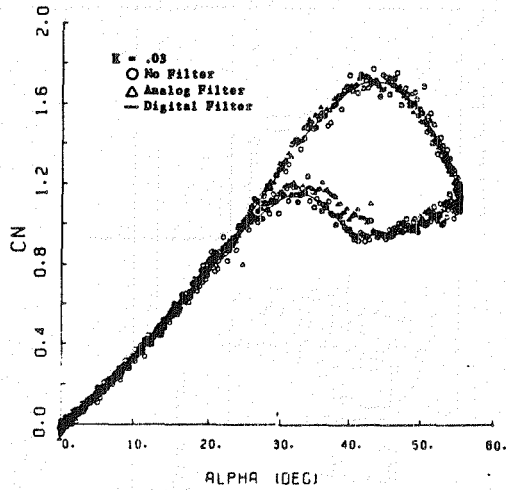


FIGURE 6. COMPARISON OF THE FILTERED AND UNFILTERED DATA.

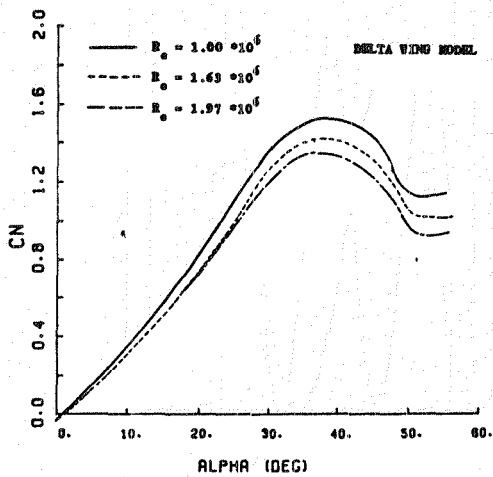


FIGURE 7. EFFECT OF REYNOLDS NUMBER ON STATIC NORMAL FORCE COEFFICIENT ($\beta = 0$).

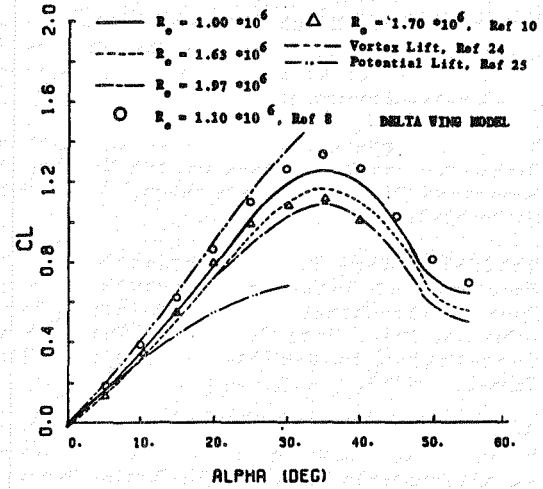


FIGURE 8. EFFECT OF REYNOLDS NUMBER ON STATIC LIFT COEFFICIENT AND COMPARISON TO OTHER EXPERIMENTS AND THEORY ($\beta = 0$).

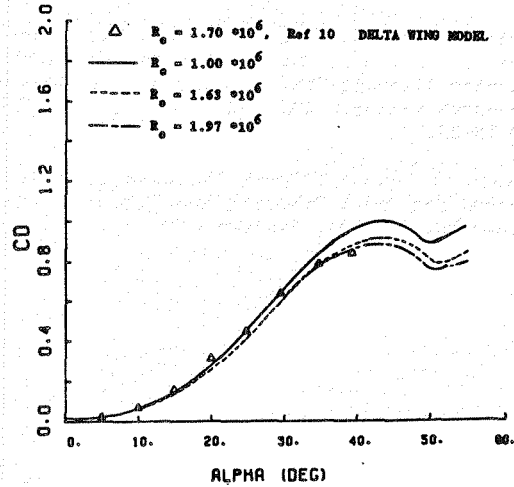


FIGURE 9. EFFECT OF REYNOLDS NUMBER ON STATIC DRAG COEFFICIENT ($\beta = 0$).

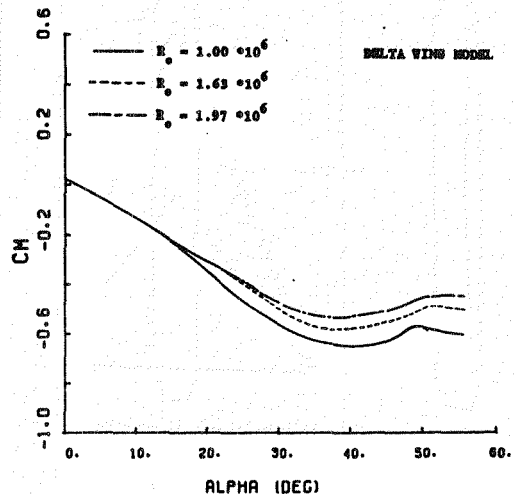


FIGURE 10. EFFECT OF REYNOLDS NUMBER ON STATIC PITCHING MOMENT COEFFICIENT ($\beta = 0$).

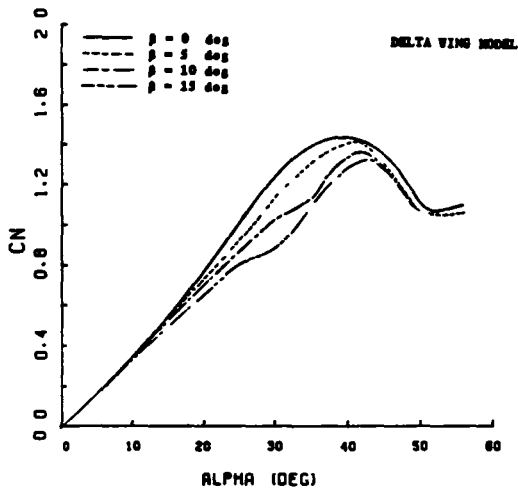


FIGURE 11. EFFECT OF SIDESLIP ON STATIC NORMAL FORCE COEFFICIENT.

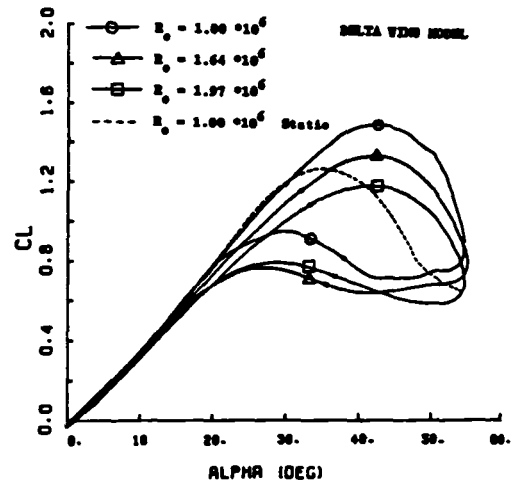


FIGURE 14. EFFECT OF REYNOLDS NUMBER ON DYNAMIC LIFT COEFFICIENT ($K = .074$).

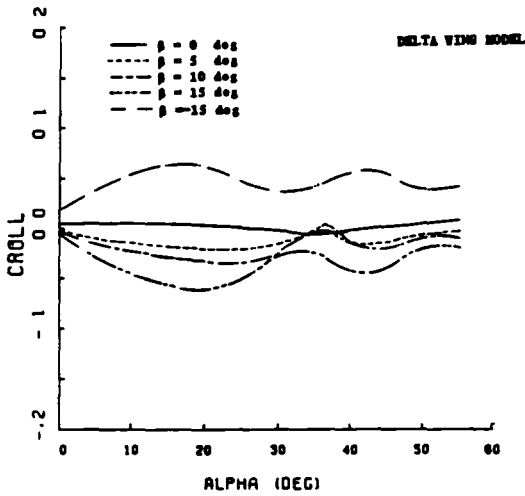


FIGURE 12. EFFECT OF SIDESLIP ON STATIC ROLLING MOMENT COEFFICIENT.

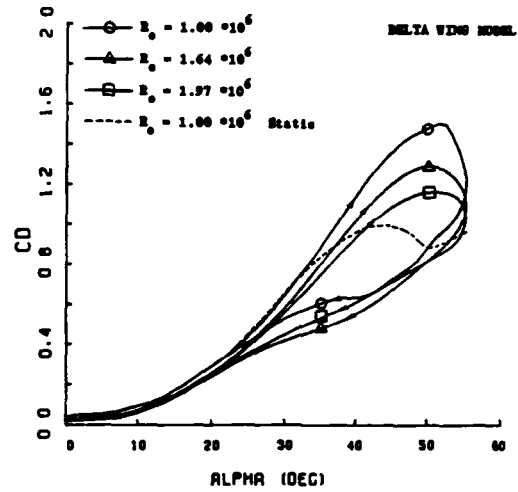


FIGURE 15. EFFECT OF REYNOLDS NUMBER ON DYNAMIC DRAG COEFFICIENT ($K = .074$).

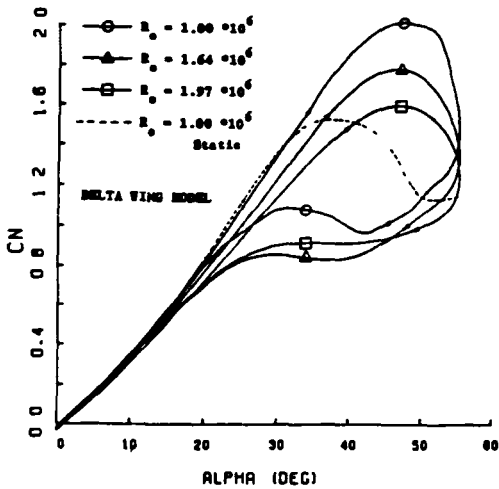


FIGURE 13. EFFECT OF REYNOLDS NUMBER ON DYNAMIC NORMAL FORCE COEFFICIENT ($K = .074$).

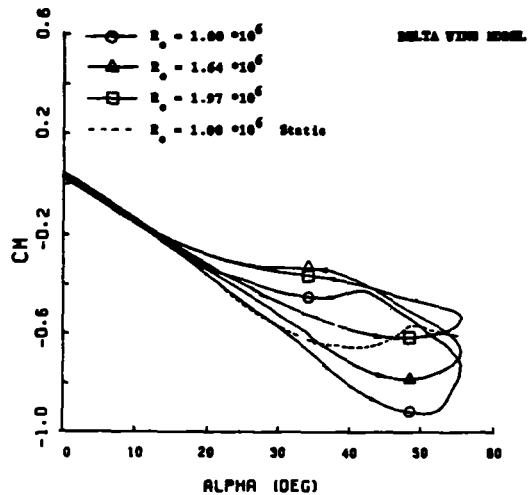


FIGURE 16. EFFECT OF REYNOLDS NUMBER ON DYNAMIC PITCHING MOMENT COEFFICIENT ($K = .074$).

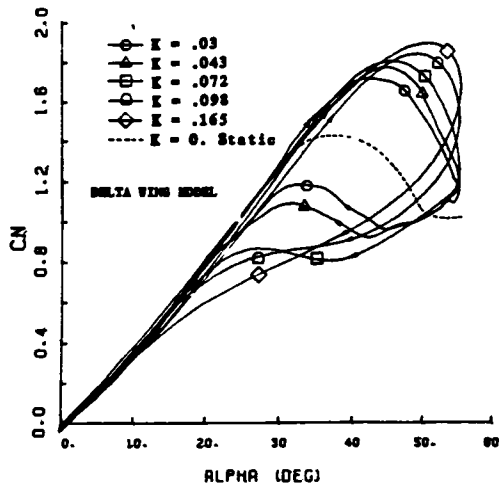


FIGURE 17. EFFECT OF REDUCED FREQUENCY ON NORMAL FORCE ($R_0 = 1.64 \times 10^6$, $\beta = 0$ deg).

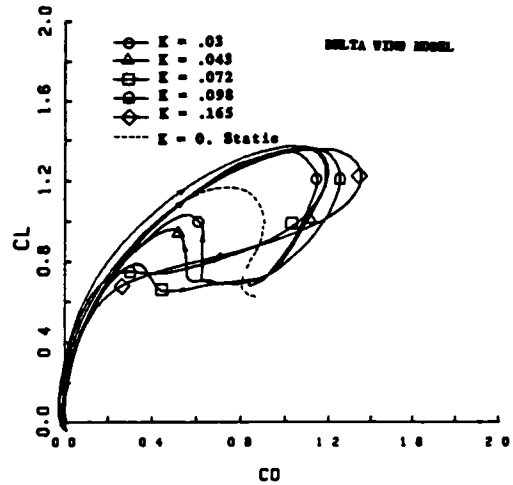


FIGURE 20. EFFECT OF REDUCED FREQUENCY ON DRAG DUE TO LIFT ($R_0 = 1.64 \times 10^6$, $\beta = 0$ deg).

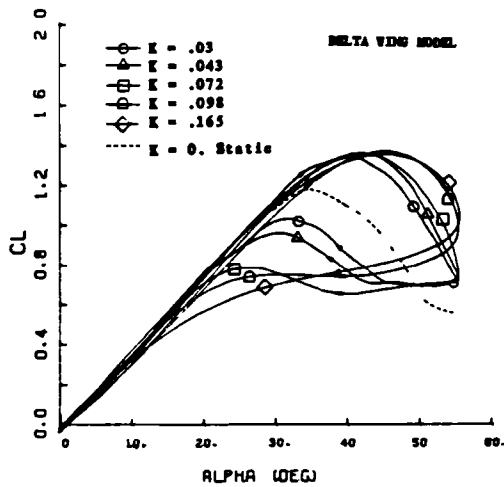


FIGURE 18. EFFECT OF REDUCED FREQUENCY ON LIFT ($R_0 = 1.64 \times 10^6$, $\beta = 0$ deg).

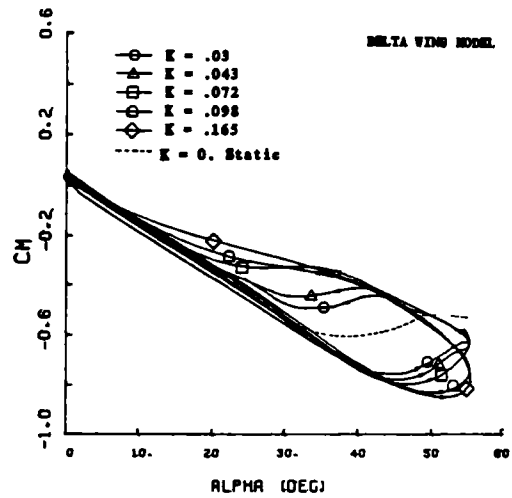


FIGURE 21. EFFECT OF REDUCED FREQUENCY ON PITCHING MOMENT ($R_0 = 1.64 \times 10^6$, $\beta = 0$ deg).

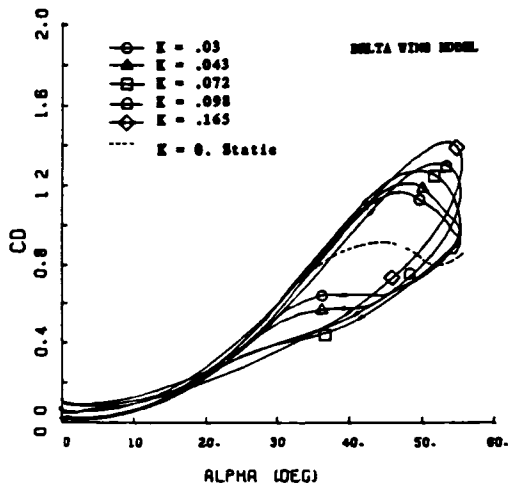


FIGURE 19. EFFECT OF REDUCED FREQUENCY ON DRAG ($R_0 = 1.64 \times 10^6$, $\beta = 0$ deg).

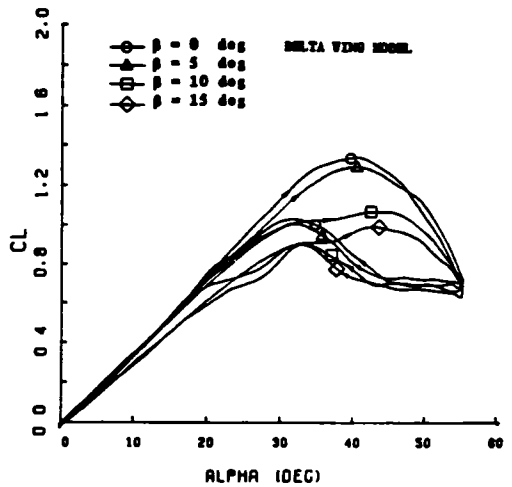


FIGURE 22. EFFECT OF SIDESLIP ON DYNAMIC LIFT COEFFICIENT ($K = .043$).

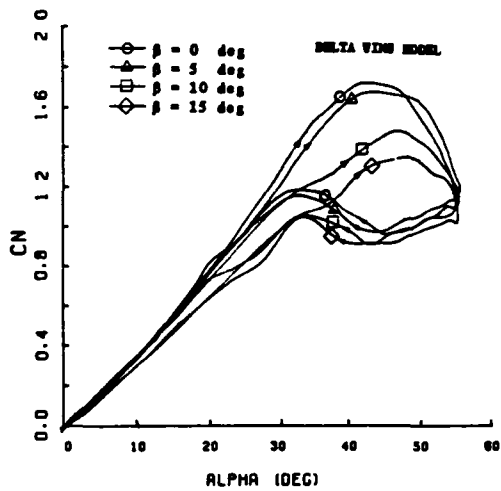


FIGURE 23. EFFECT OF SIDESLIP ON DYNAMIC NORMAL FORCE COEFFICIENT ($K = .043$).

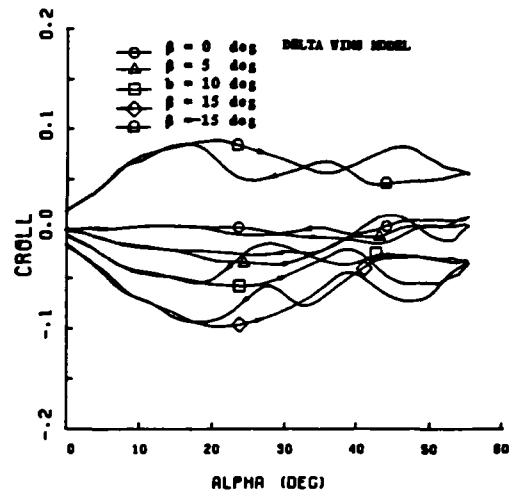


FIGURE 26. EFFECT OF SIDESLIP ON DYNAMIC ROLLING MOMENT COEFFICIENT ($K = .043$).

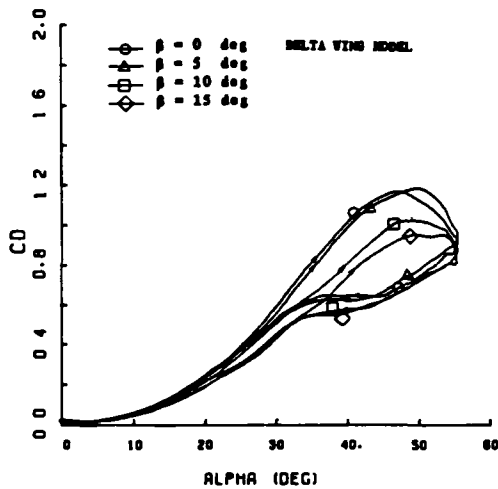


FIGURE 24. EFFECT OF SIDESLIP ON DYNAMIC DRAG COEFFICIENT ($K = .043$).

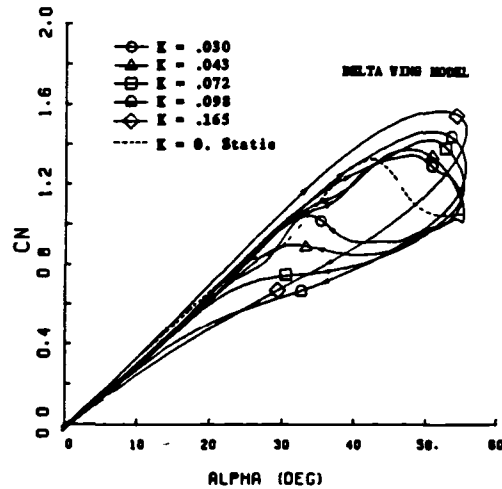


FIGURE 27. EFFECT OF REDUCED FREQUENCY ON NORMAL FORCE ($Re = 1.64 \cdot 10^6$, $\beta = 15$ deg).

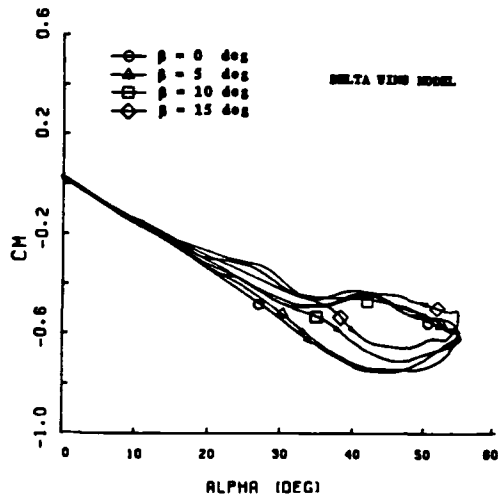


FIGURE 25. EFFECT OF SIDESLIP ON DYNAMIC PITCHING MOMENT COEFFICIENT ($K = .043$).

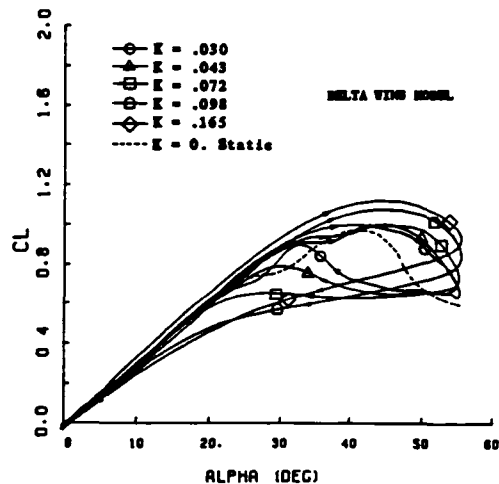


FIGURE 28. EFFECT OF REDUCED FREQUENCY ON LIFT FORCE ($Re = 1.64 \cdot 10^6$, $\beta = 15$ deg).

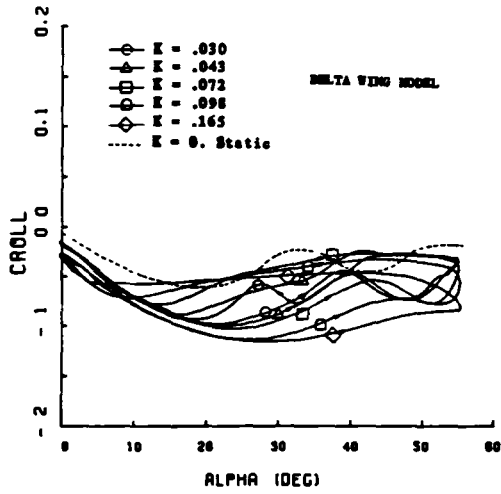


FIGURE 29. EFFECT OF REDUCED FREQUENCY ON ROLLING MOMENT ($Re = 1.64 \cdot 10^6$, $\beta = 15$ deg).

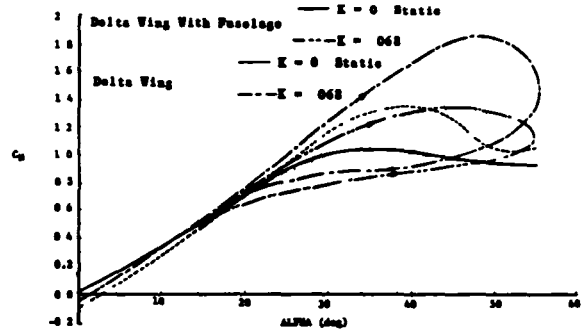


FIGURE 30. COMPARISON OF NORMAL FORCE DATA ON BOTH MODELS ($\beta = 0$).

APPENDIX B



**Aeronautical and Astronautical
Research Laboratory**

2300 West Case Road
Columbus, OH 43220-1949
Phone 614-292-5491

**EXPERIMENTAL MEASUREMENTS ON AN OSCILLATING
70-DEGREE DELTA WING IN SUBSONIC FLOW**

M. B. BRAGG

M. R. SOLTANI

**THE OHIO STATE UNIVERSITY
COLUMBUS, OHIO**

presented to

**NASA LANGLEY RESEARCH CENTER
DECEMBER 10, 1987**

*** FUNDED BY NASA LANGLEY
GRANT NAG-1-641**

INTRODUCTION

- **OBJECTIVE**

TO BETTER UNDERSTAND THE FLOW FIELD AND THE RESULTING FORCES AND MOMENTS ON DELTA WINGS AND OTHER THREE-DIMENSIONAL HIGH PERFORMANCE AIRCRAFT CONFIGURATIONS UNDER DYNAMIC, HIGH ANGLE OF ATTACK ENVIRONMENTS.

- **CURRENT APPROACH**

USE EXPERIMENTAL MEASUREMENTS OF FORCES AND MOMENTS AS WELL AS FLOW VISUALIZATION TO STUDY THE FLOW ABOUT A DELTA WING OSCILLATING IN PITCH ($\alpha + \dot{\theta}$) IN SUBSONIC FLOW.



OUTLINE

- INTRODUCTION
- DELTA WING MODELS, OSCILLATION SYSTEM AND THE WIND TUNNEL
- DATA ACQUISITION AND REDUCTION
- FORCE DATA, WITH AND WITHOUT FUSELAGE, $\beta = 0$
- FORCE DATA, WITHOUT FUSELAGE, $\beta = -15$ TO 15 DEGREES
- FLOW VISUALIZATION



MODELS, OSCILLATION SYSTEM AND TUNNEL

● 70-DEGREE DELTA WING MODELS:

MODEL WITH FUSELAGE - "LOW WING", CYNINDRICAL FUSELAGE, ALL
COMPOSITE, b = 12 inches

MODEL WITHOUT FUSELAGE - BALANCE POD ON LOWER SURFACE,
PLYWOOD, b = 15 inches

● OSCILLATION SYSTEM:

CAM DRIVEN - AOA= 0 TO 55 DEG, F= 0 TO 2.5 HZ

CURRENT CAM - SINUSOIDAL AOA

● TUNNEL:

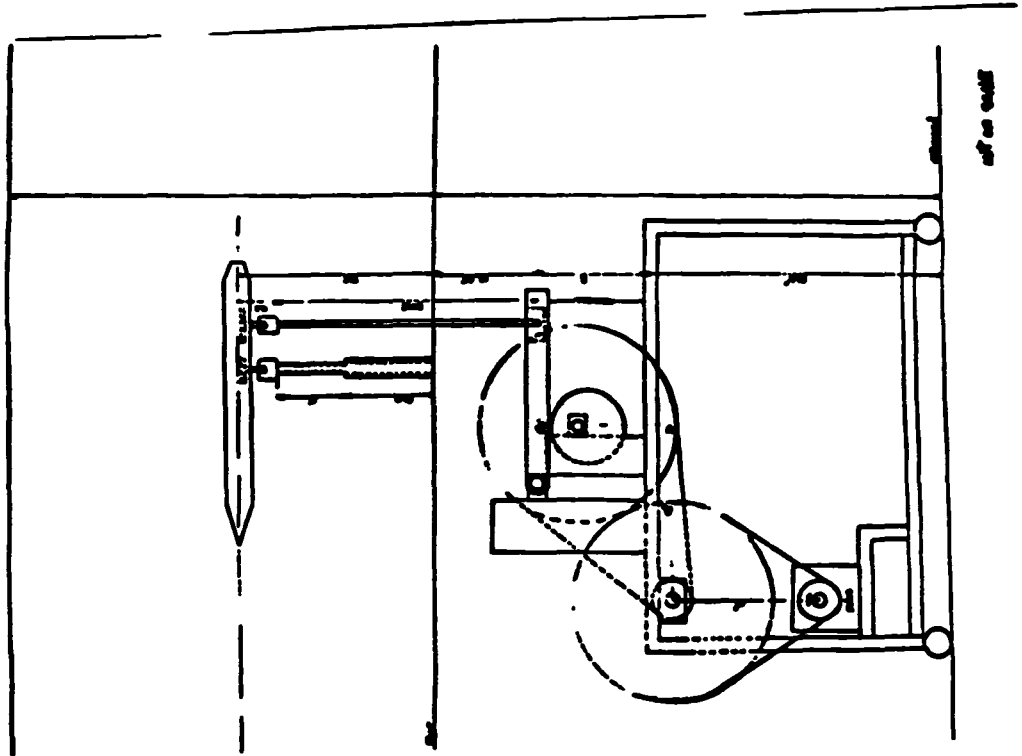
TEST SECTION - 3 X 5 X 8 FEET

SPEED - 0 TO 200 FT/SEC

TURBULENCE - 0.15 PERCENT



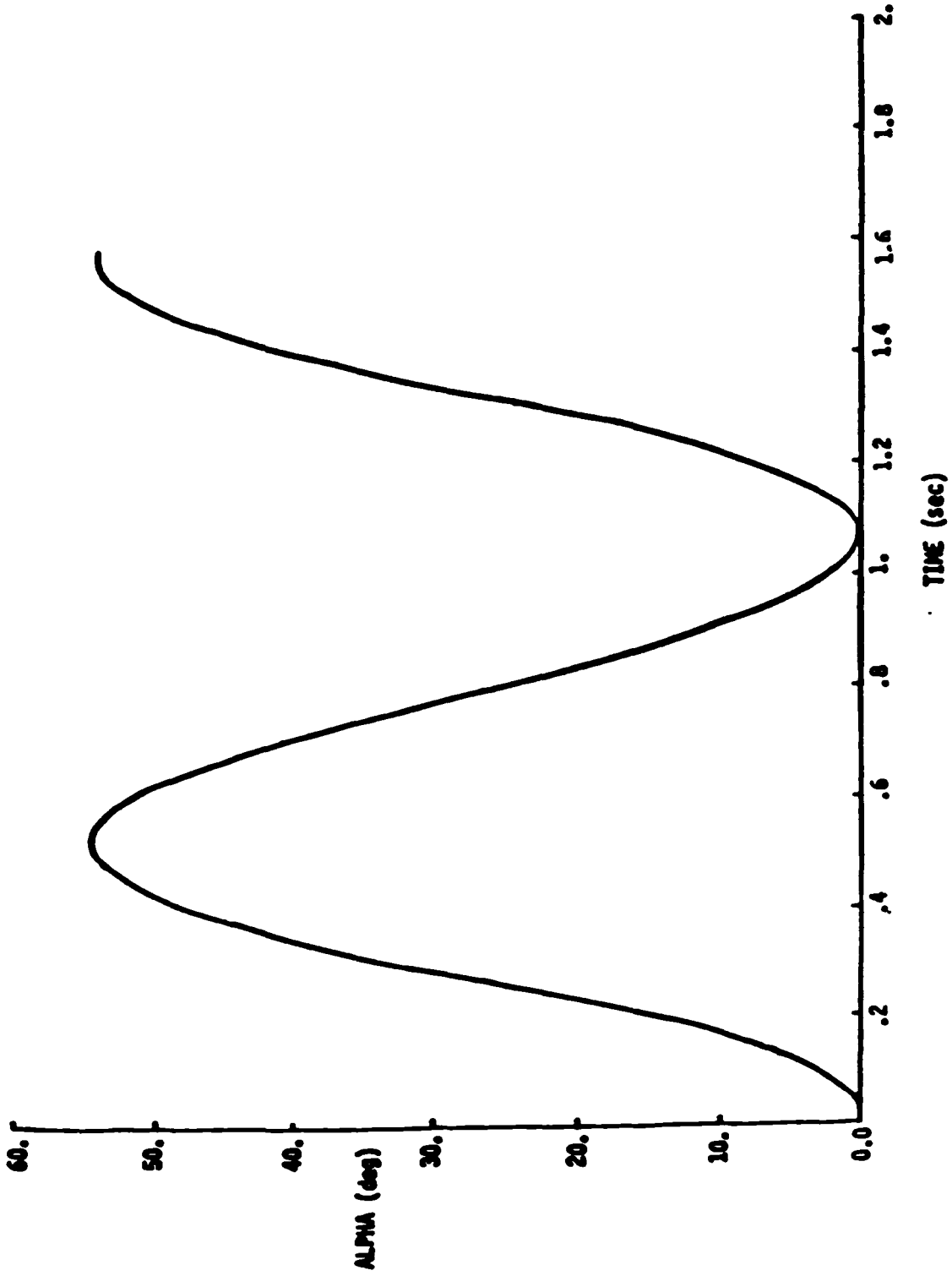
OSCILLATING SYSTEM



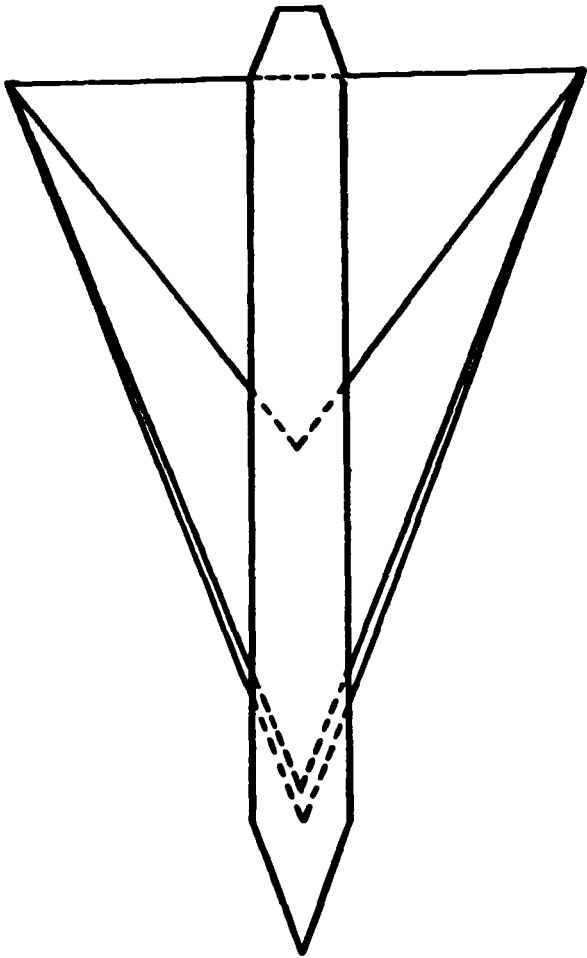
of an oscill



ANGLE OF ATTACK (deg) vs TIME (sec) FREQ = 0.94hz



12.0"



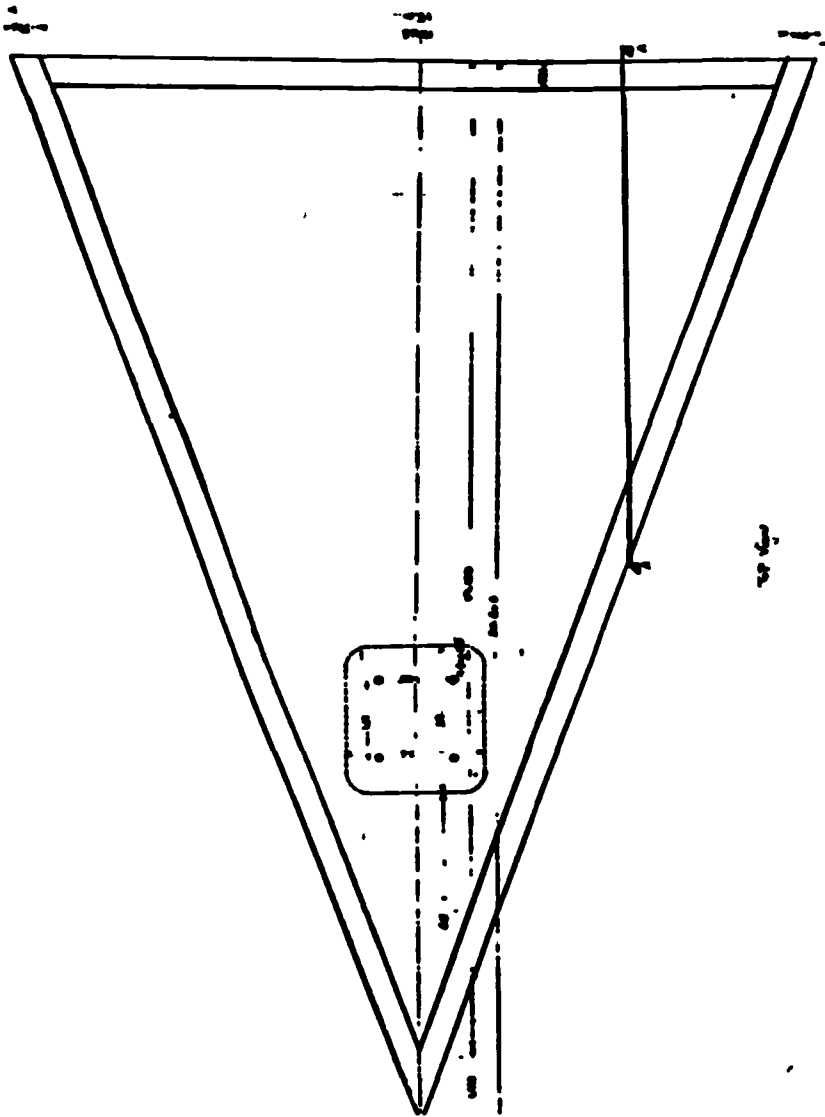
3.6"
16.485"
21.0"



DELTA WING MODEL



DELTA WING



Wing Section



Wing Section

Wing Section



Wing Section

DATA ACQUISITION

- IBM PC/XT WITH DATA TRANSLATION 12-BIT, 16-CHANNEL A TO D ,
- SIX-COMPONENT, INTERNAL STRAIN GAUGE BALANCE SUPPLIED BY NASA LANGLEY
- SAMPLING 11 CHANNELS AT 600 TO 1000 HZ
 - 6 BALANCE CHANNELS
 - 2 TUNNEL SPEED TRANSDUCERS
 - 1 HOT WIRE FOR TUNNEL SPEED
 - 2 ANGLE OF ATTACK POTENTIOMETERS



DATA REDUCTION

- DATA CORRECTIONS - NEW SET TAKEN BEFORE EACH SERIES OF RUNS
 - BALANCE ZEROS
 - GRAVITY TARES VS AOA
model and balance
 - DYNAMIC TARES VS AOA (OR THE INSTANTANEOUS DERIVATIVES)
model and balance

- COORDINATE SYSTEMS
 - LONGITUDINAL FORCES AND MOMENTS - WIND AXIS SYSTEM
 - LATERAL FORCES AND MOMENTS - BODY AXIS SYSTEM

- NEAR REAL TIME REDUCTION ON THE IBM PC/XT
 - TABULATED AND PLOTTED $C_N, C_A, C_M ; C_Y, C_N, C_l$ VS AOA OR t

- POST PROCESSOR ON THE HARRIS H800
 - ALL DATA STORED IN DIRECT ACCESS FILES
 - MAKES COMPOSITE PLOTS
 - FUTURE PLANS - DIGITAL FILTERING, ENSEMBLE AVERAGING AND STABILITY DERIVATIVES



10-05-1987

ONLINE DATA REDUCTION

14:56:55

Run # 81
Ine-10DC
600,400
 $\beta = -15$

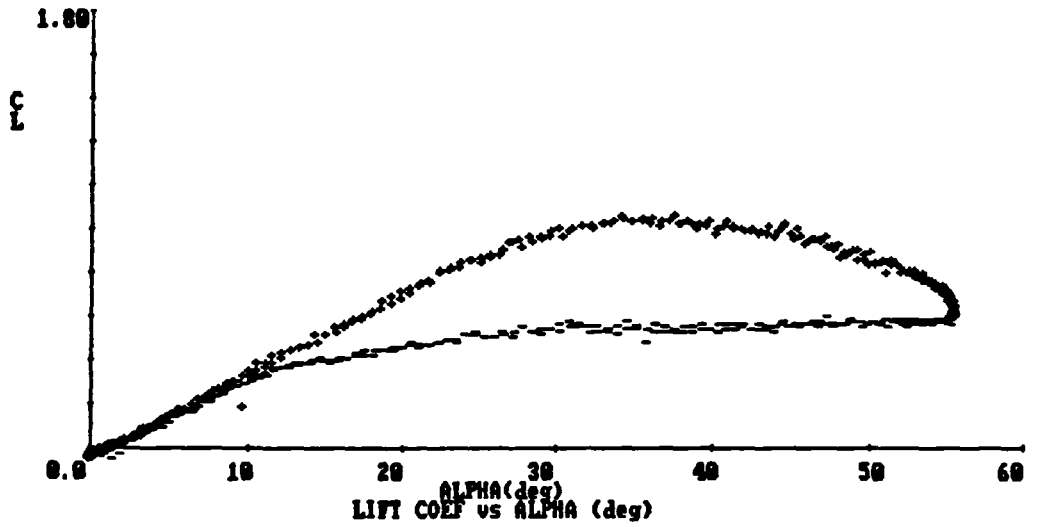
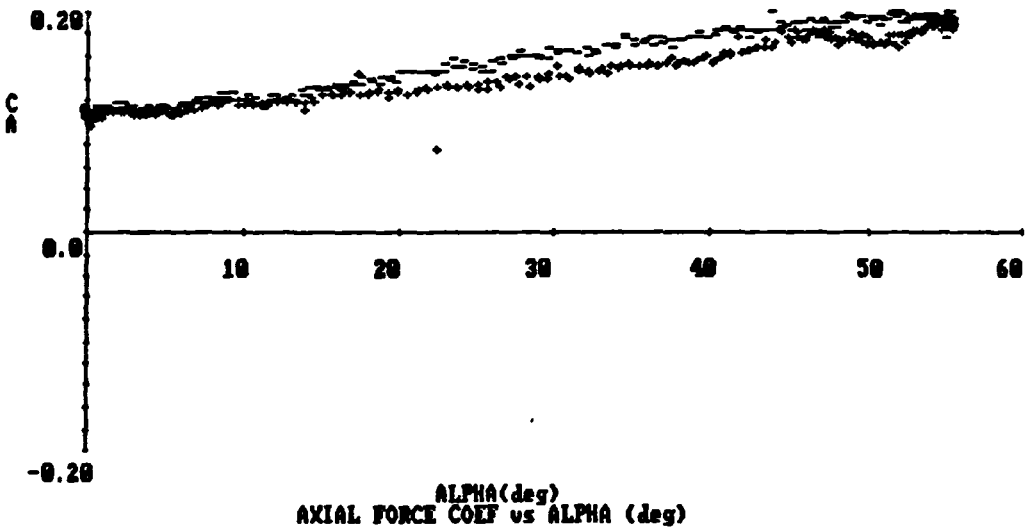
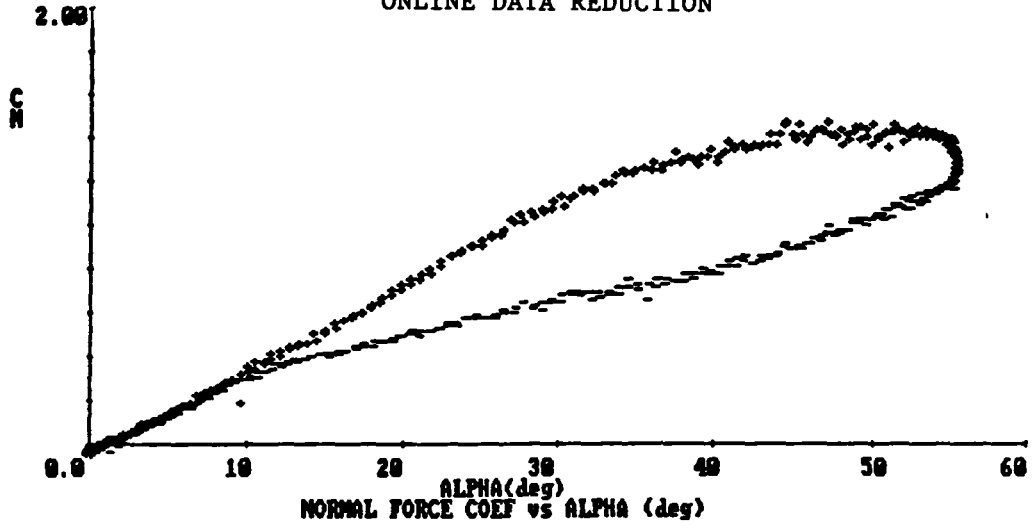
AERODYNAMIC LOADS WHEN MODEL IS OSCILLATING (TUNNEL ON)

SIDESLIP ANGLE = -15 deg

ALPHA(deg)	VEL (ft/sec)TR	CL	Cd	Cm	Cy	Cn	Cl
.1356484	143.9601	-3.403437E-02	.1133796	5.548602E-02	-2.812392E-02	-5.88823E-03	2.185299E-03
-0.153766E-02	143.8422	-3.436278E-02	.1180125	5.993446E-02	-3.396207E-02	-8.963333E-03	3.841355E-04
-1.898981	143.6146	-3.737197E-02	.1198758	5.914879E-02	-3.824516E-02	-1.198163E-02	1.135126E-03
.0812781	146.2931	-4.426305E-02	.1115959	5.342422E-02	-.0428694	-1.698589E-02	1.949487E-03
.788488	146.0251	3.150726E-03	.1895359	3.276822E-02	-3.361863E-02	-1.415837E-02	5.388355E-03
1.587416	147.1373	1.177874E-02	.1115677	2.723763E-02	-2.617510E-02	-8.688174E-03	1.012778E-02
2.99918	146.1313	6.258182E-02	.112031	-1.932267E-03	-2.271847E-02	-5.331518E-03	1.733243E-02
4.697186	144.247	.1239092	.1179576	-3.440476E-02	-7.980621E-02	2.185904E-03	2.552873E-02
6.732585	142.054	.2832192	.134554	-7.491661E-02	8.072466E-03	1.075885E-02	3.968542E-02
8.959372	145.3184	.2789486	.1548803	-.1137859	1.592672E-02	1.608617E-02	4.932815E-02
11.53946	144.5798	.3783363	.1859383	-.1689706	1.997294E-02	1.780852E-02	6.823942E-02
14.44531	148.2489	.4295487	.2154184	-.1884104	.0382317	.0238585	6.473683E-02
17.29838	146.3497	.5348755	.2934529	-.2413338	4.858765E-02	2.577554E-02	7.331658E-02
20.4171	145.9472	.6379846	.3443217	-.2845988	.0545329	2.583804E-02	7.577878E-02
23.62112	144.8827	.7455131	.4375195	-.3455365	6.544694E-02	3.017559E-02	8.134224E-02
26.89086	143.1437	.8472295	.5488912	-.4061768	7.583936E-02	3.521056E-02	8.812974E-02
30.14215	143.4882	.8997274	.6558625	-.4513981	6.781364E-02	3.386159E-02	7.582455E-02
33.48846	145.9803	.916813	.7324557	-.4873946	6.269388E-02	3.147332E-02	7.118222E-02
36.48635	145.9844	.912267	.8181813	-.5146381	5.896973E-02	3.031752E-02	6.216398E-02
39.45656	145.1113	.9127143	.9099162	-.5597655	4.583272E-02	2.664546E-02	5.629415E-02
42.28593	144.848	.8883921	.9982519	-.5928835	2.268819E-02	2.339614E-02	5.181385E-02
44.85987	143.8556	.8788834	1.078746	-.6423388	2.788244E-02	2.994439E-02	5.552296E-02
47.05527	141.7413	.8651174	1.151108	-.6812972	2.748485E-02	2.833745E-02	5.977152E-02
49.14554	143.8458	.8152499	1.168667	-.6812134	.0193182	2.167604E-02	6.884223E-02
50.98481	145.5474	.7176298	1.189783	-.6274848	1.556895E-02	1.795758E-02	6.823813E-02
52.48899	144.4781	.7247847	1.186267	-.6666684	3.076651E-02	2.681218E-02	6.859157E-02
53.67685	143.8384	.6762286	1.182399	-.653174	3.386585E-02	3.194711E-02	6.233978E-02
54.65257	143.6441	.6732114	1.171657	-.6364929	2.881735E-02	3.054636E-02	5.568375E-02
55.28478	142.147	.596757	1.165182	-.6384479	3.842369E-02	3.188959E-02	5.483821E-02
55.39855	142.3184	.5882874	1.127895	-.6189911	2.133988E-02	2.28827E-02	4.622995E-02
55.42782	142.6176	.5548826	1.091314	-.5876691	2.317978E-02	2.469631E-02	4.726467E-02
54.72576	142.6941	.5384198	1.042869	-.5591239	2.282333E-02	2.649957E-02	4.176887E-02
53.9636	142.7857	.5124252	.9962466	-.5313655	.0338778	.0326639	3.999439E-02
52.96889	143.3788	.5039913	.9584249	-.5088673	2.288747E-02	.0266821	3.398865E-02
51.44687	142.3662	.5154977	.9286358	-.4989392	.0238564	.0265772	3.628587E-02
49.88286	142.767	.518935	.864681	-.4556888	2.424481E-02	2.565933E-02	3.321725E-02
47.85871	143.5653	.589985	.886326	-.4284813	2.336991E-02	2.733881E-02	.0386895
45.76222	142.1786	.5837648	.7683639	-.3984672	1.868386E-02	.025583	2.928489E-02
43.32151	143.1221	.4916275	.6987354	-.358339	3.071889E-03	1.636793E-02	1.819941E-02
40.88562	143.1948	.4918847	.6399583	-.332663	.0123519	1.019941E-02	1.341994E-02
38.85629	144.222	.4739683	.5694484	-.2939122	5.693527E-03	1.341994E-02	1.529553E-02
35.84244	147.6239	.4819689	.4797418	-.2724581	7.72357E-03	1.529553E-02	1.884246E-02
32.88718	143.7355	.4773589	.4272627	-.2498188	-2.941773E-03	1.884246E-02	1.522832E-02
28.98597	143.6818	.4616189	.4231746	-.2284887	5.036912E-03	1.522832E-02	...
25.92882	143.4353	.4682975	.3827459	-.2831891	-4.239855E-03	1.127844E-02	1.682376E-02
22.98729	143.7184	.4482533	.3358777	-.1771926	-7.197754E-03	1.018873E-02	1.448963E-02
19.9142	142.5789	.4136522	.2965157	-.1541922	-3.58483E-03	1.011635E-02	.0178732
16.9932	143.9914	.3818841	.2478981	-.1297015	7.171584E-03	1.216671E-02	2.629676E-02
14.03831	144.1246	.3535627	.2879883	-.1181575	8.967241E-03	9.612357E-03	3.516625E-02
11.45825	148.7528	.3269744	.194847	-.1075182	1.244517E-02	9.794185E-03	4.827755E-02



ONLINE DATA REDUCTION



RUNS COMPLETED AS OF 30 NOVEMBER 1987

● FUSELAGE MODEL

STATIC CASE: $\alpha = 0$ TO 55 DEG, $RE = 1.5 \times 10^6$, $\beta = 0$.

DYNAMIC CASE: $\alpha = 0$ TO 55 DEG SINUSOIDAL, $RE = 1.5 \times 10^6$
 $K = 0$. TO 0.112, $\beta = 0$ DEG

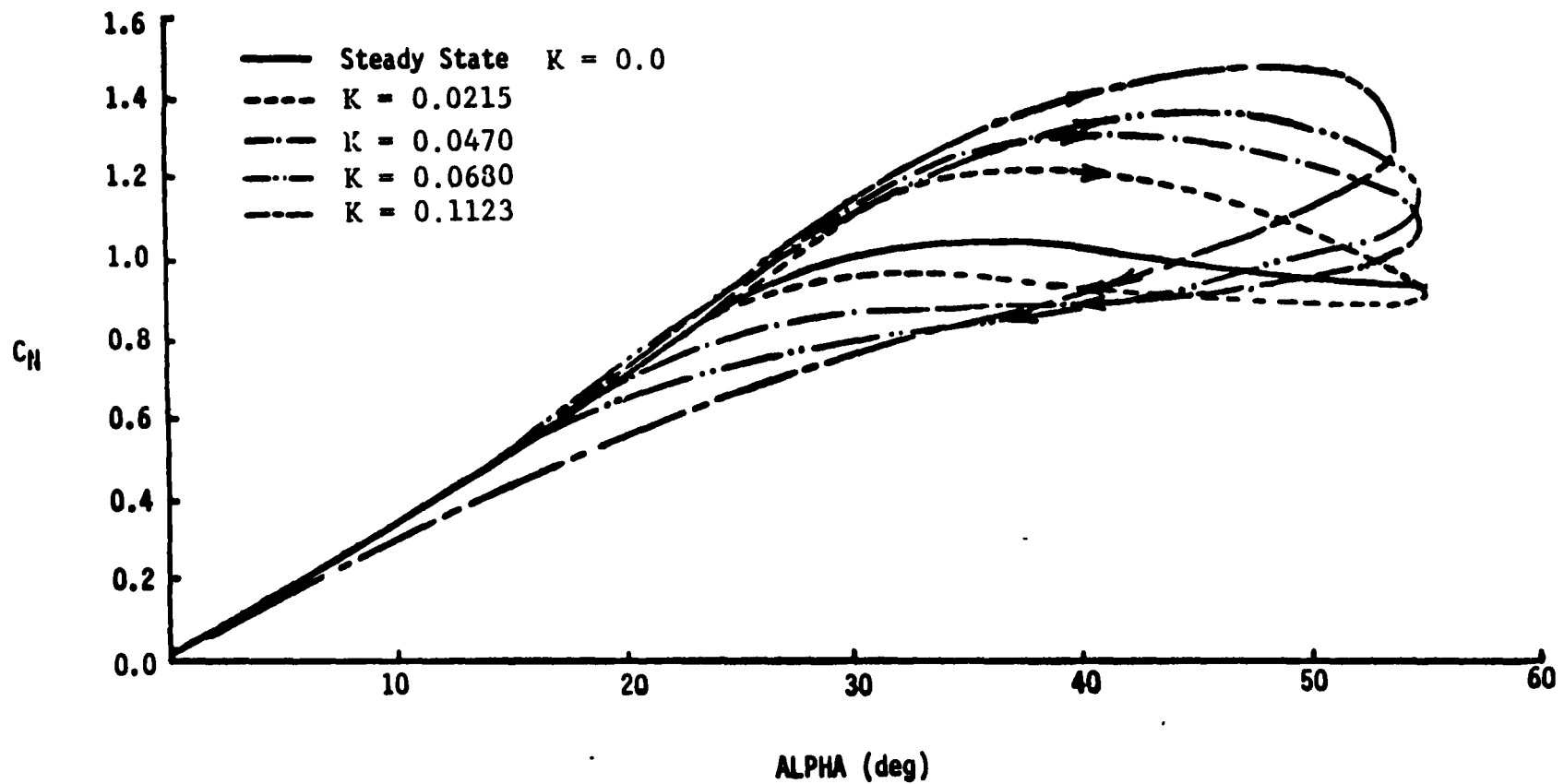
● NO FUSELAGE MODEL: (C = 20.606 IN)

STATIC CASE: $\alpha = 0$ TO 55 DEG, $RE = 6.55 \times 10^5$ TO 1.64×10^6 , $\beta = -15^\circ$ TO 15°

DYNAMIC CASE $\alpha = 0$ TO 55 DEG SINUSOIDAL, $RE = 6.55 \times 10^5$ TO
 1.64×10^6 , $K = 0.036$ TO 0.405 , $\beta = -15$ TO 15 DEG

FLOW VISUALIZATION: STATIC $\alpha = 0$ TO 55 DEG, $RE = 1.64 \times 10^6$
 $\beta = -15$ TO 15 DEG

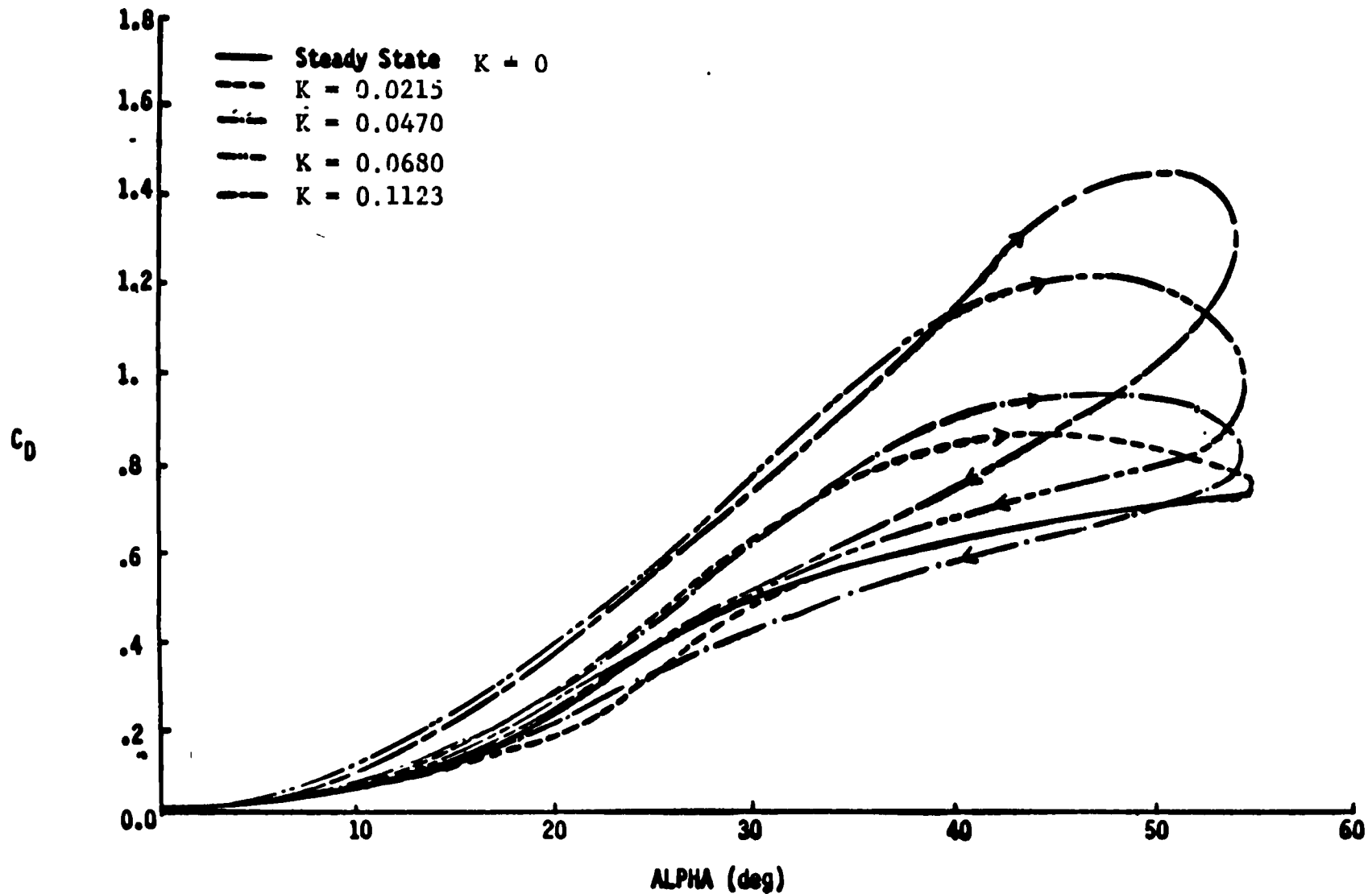




UNSTEADY AERODYNAMIC EFFECT ON NORMAL FORCE ($\beta=0$)

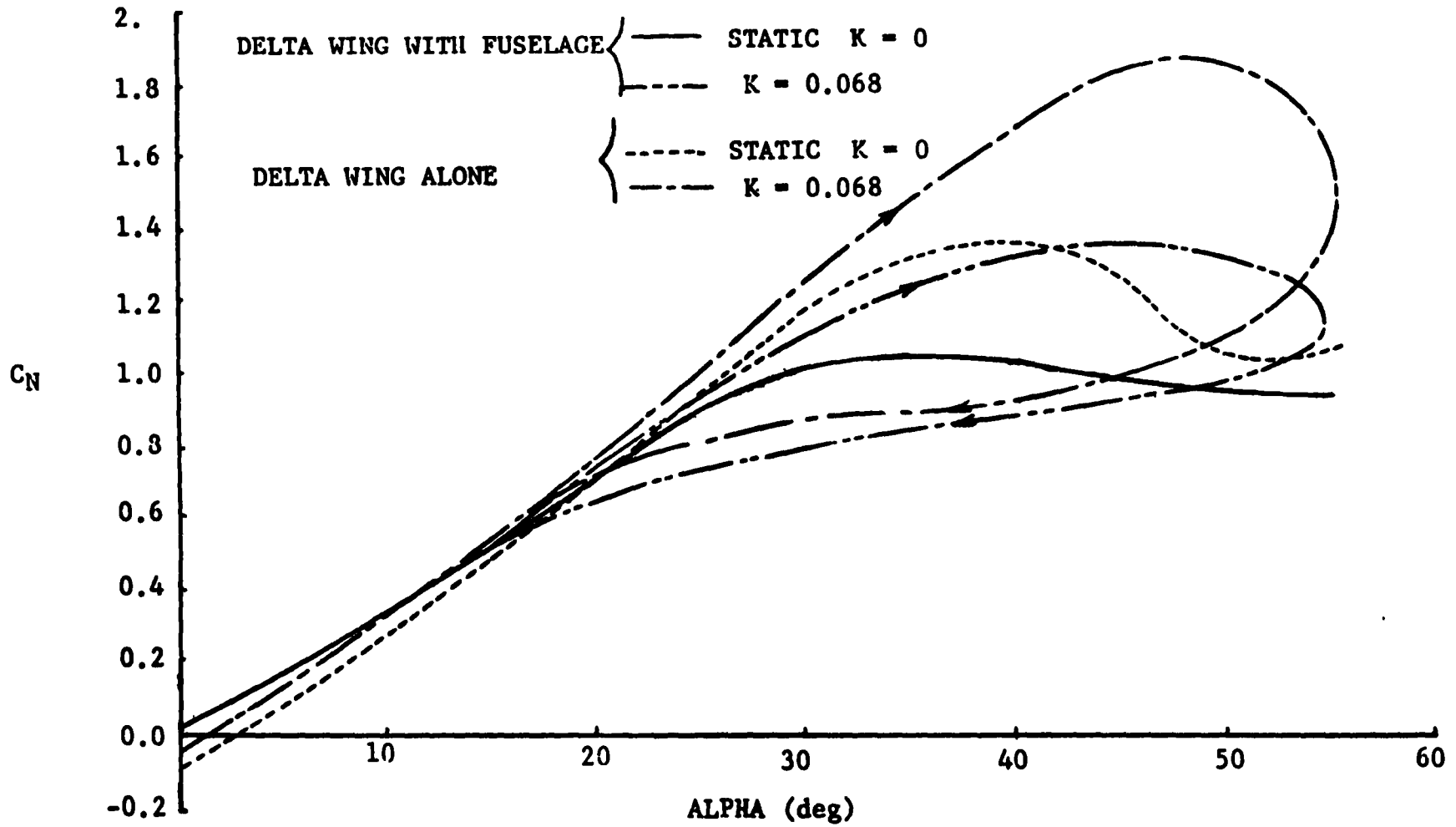
DELTA WING + BODY





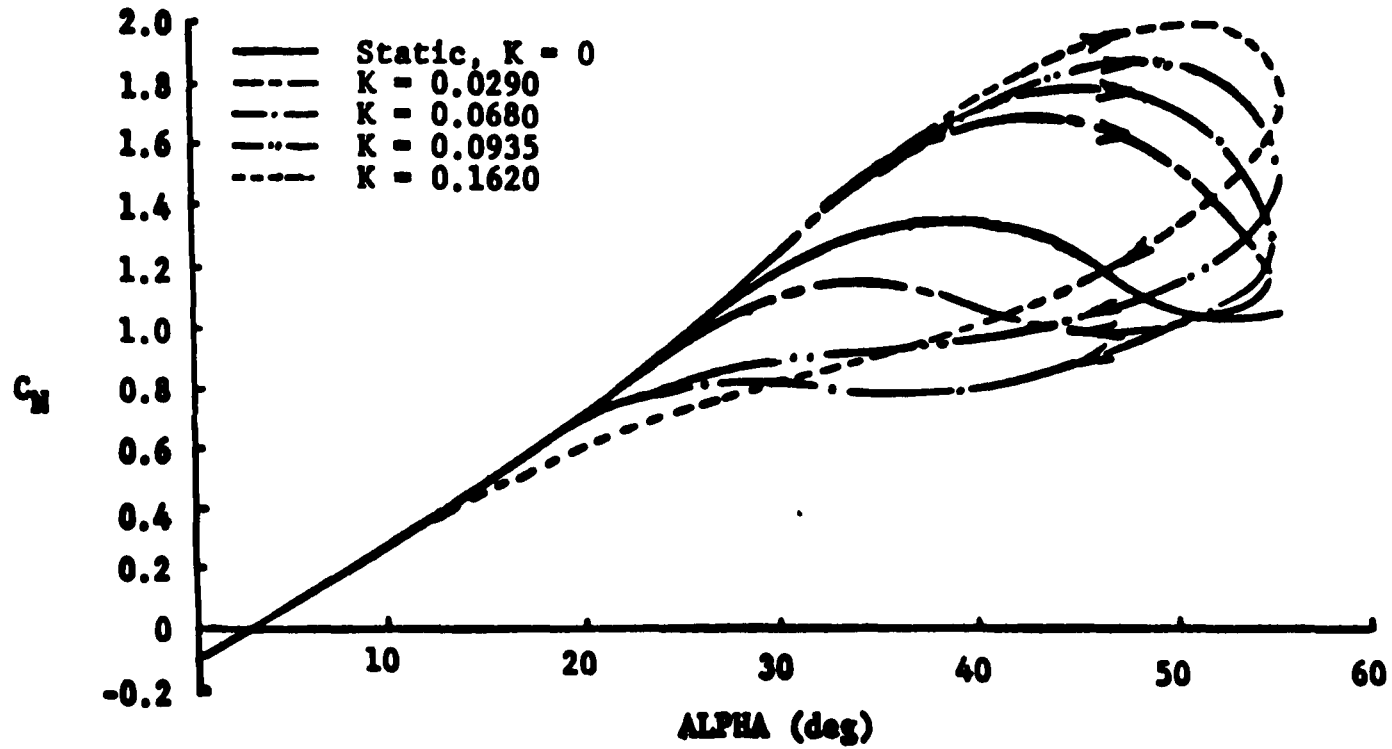
UNSTEADY AERODYNAMIC EFFECT ON DRAG ($\beta=0$)
 DELTA WING + BODY





COMPARISON OF NORMAL FORCE vs ALPHA ON BOTH MODELS ($\beta=0$)

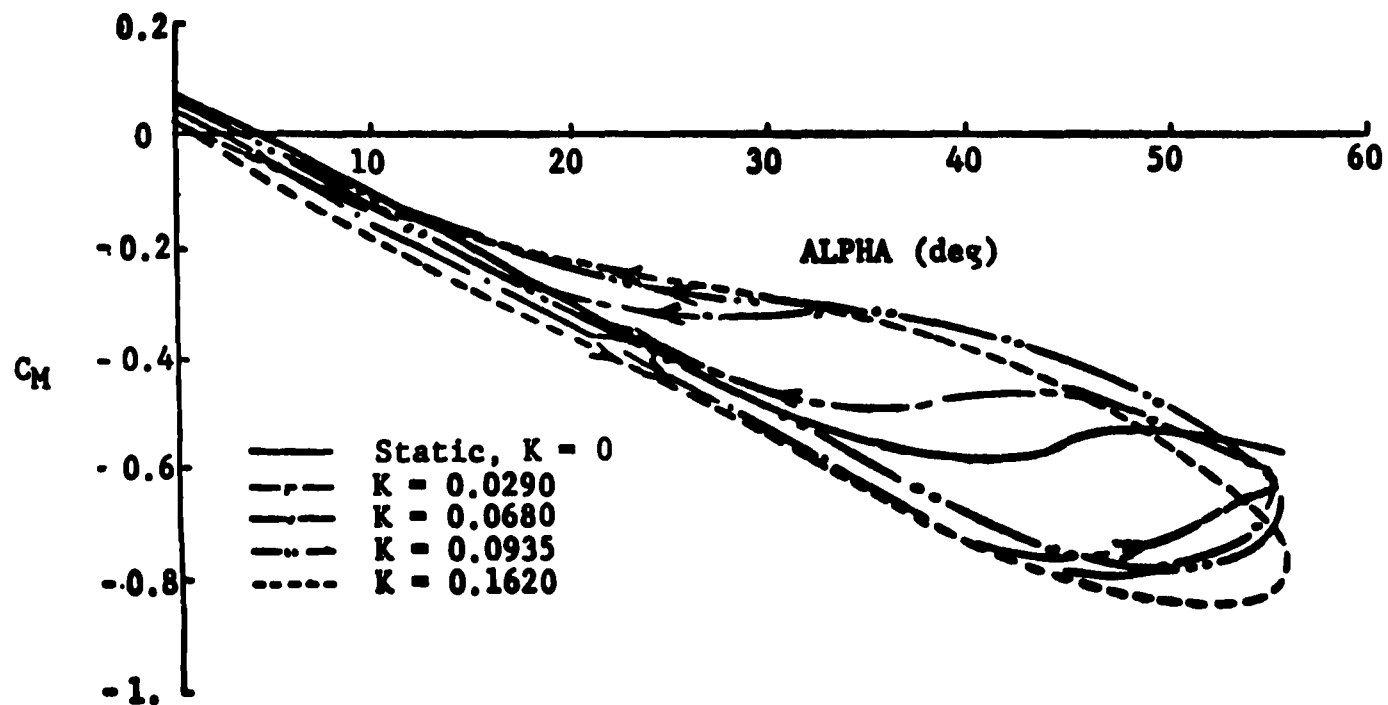




UNSTEADY AERODYNAMIC EFFECT ON NORMAL FORCE ($\beta=0$)

DELTA WING

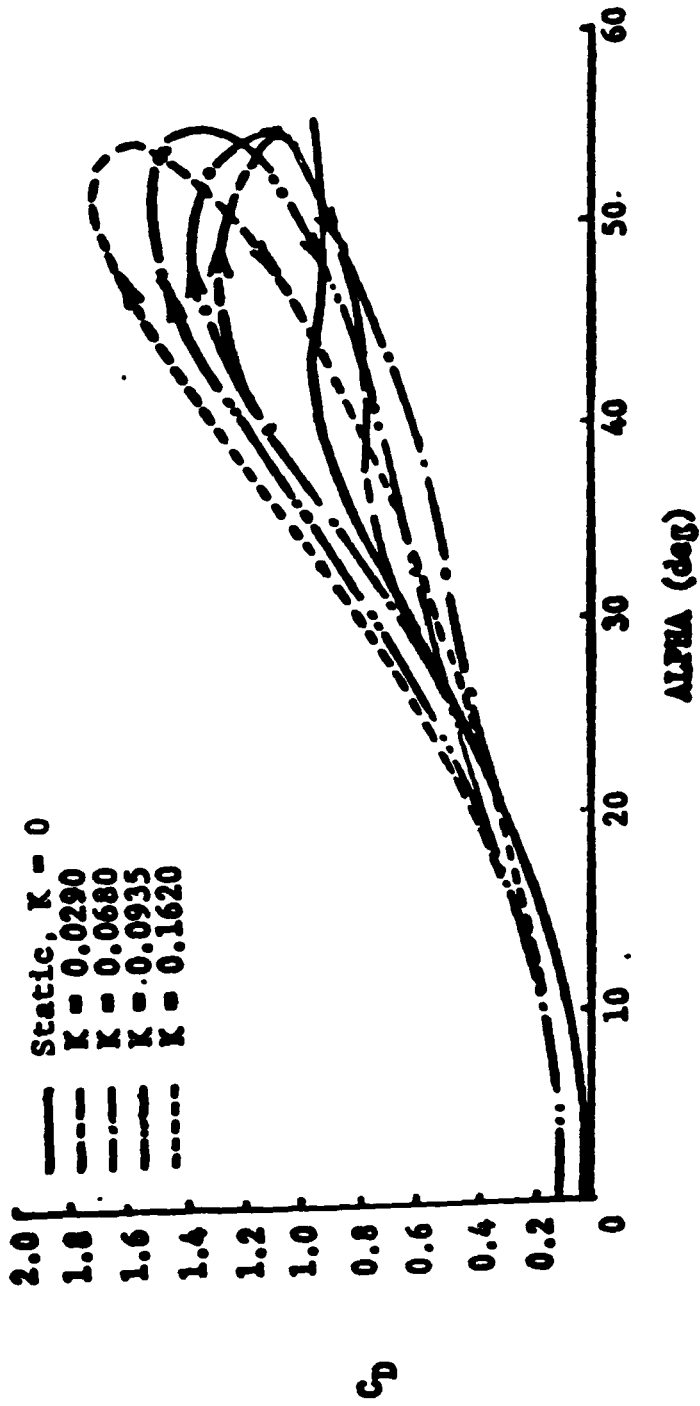




UNSTEADY AERODYNAMIC EFFECT ON PITCHING MOMENT ($\beta=0$)

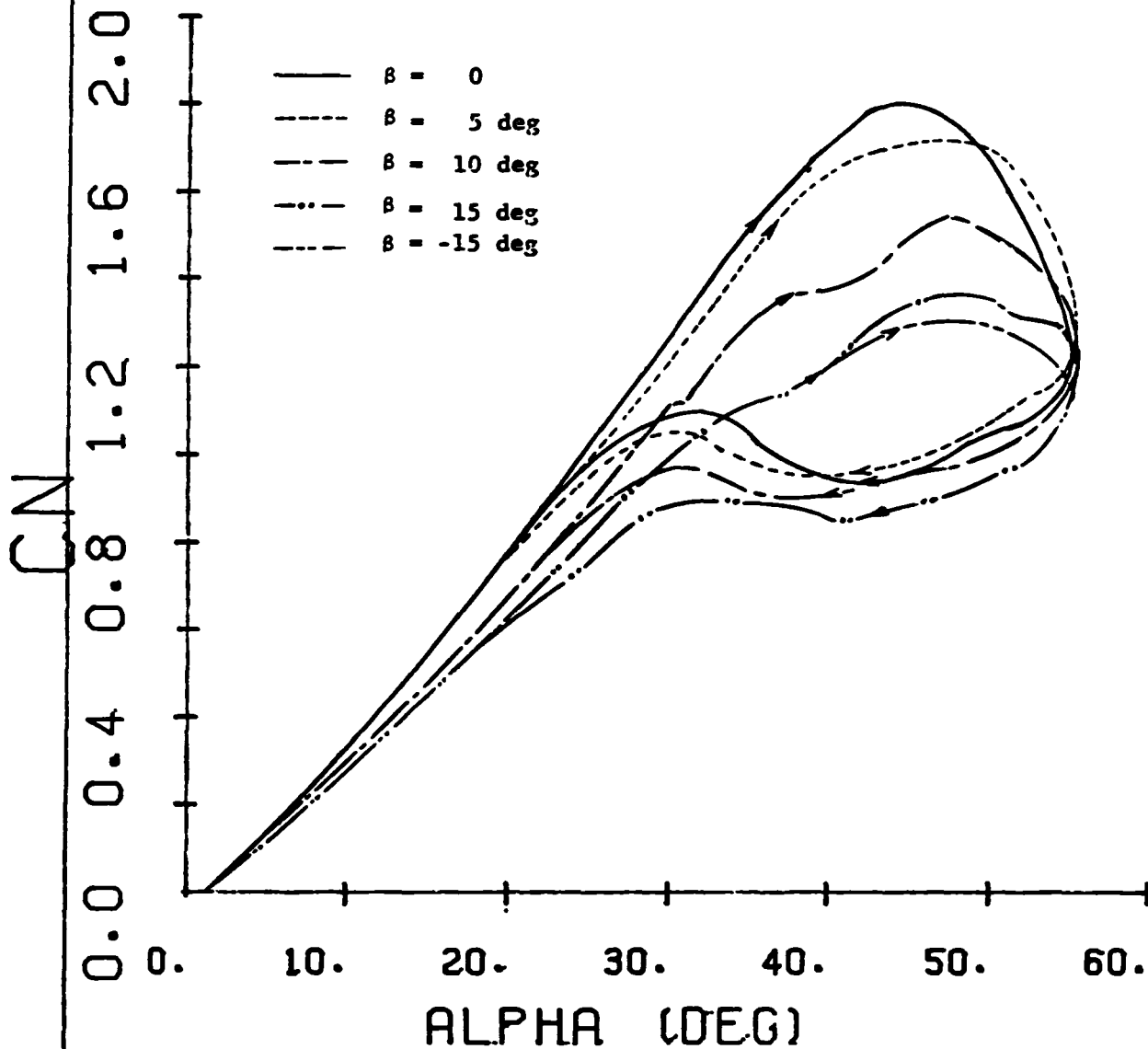
DELTA WING





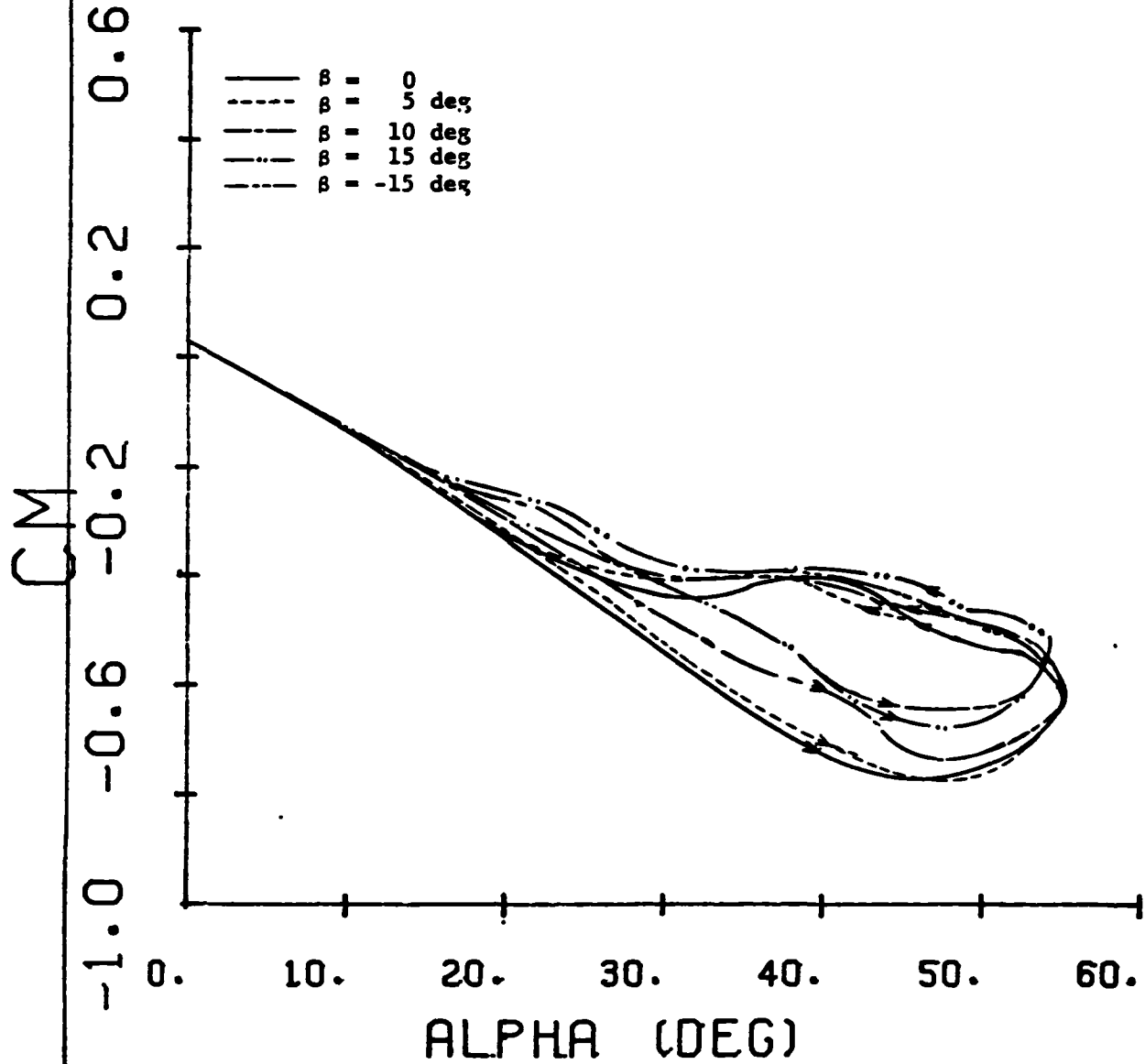
UNSTEADY AERODYNAMIC EFFECT ON DRAG ($\beta = 0$)
DELTA WING

CN VS. ALPHA



UNSTEADY AERODYNAMIC FORCE ON NORMAL FORCE VARYING SIDESLIP ANGLE
($K = 0.043$)

CM VS. ALPHA

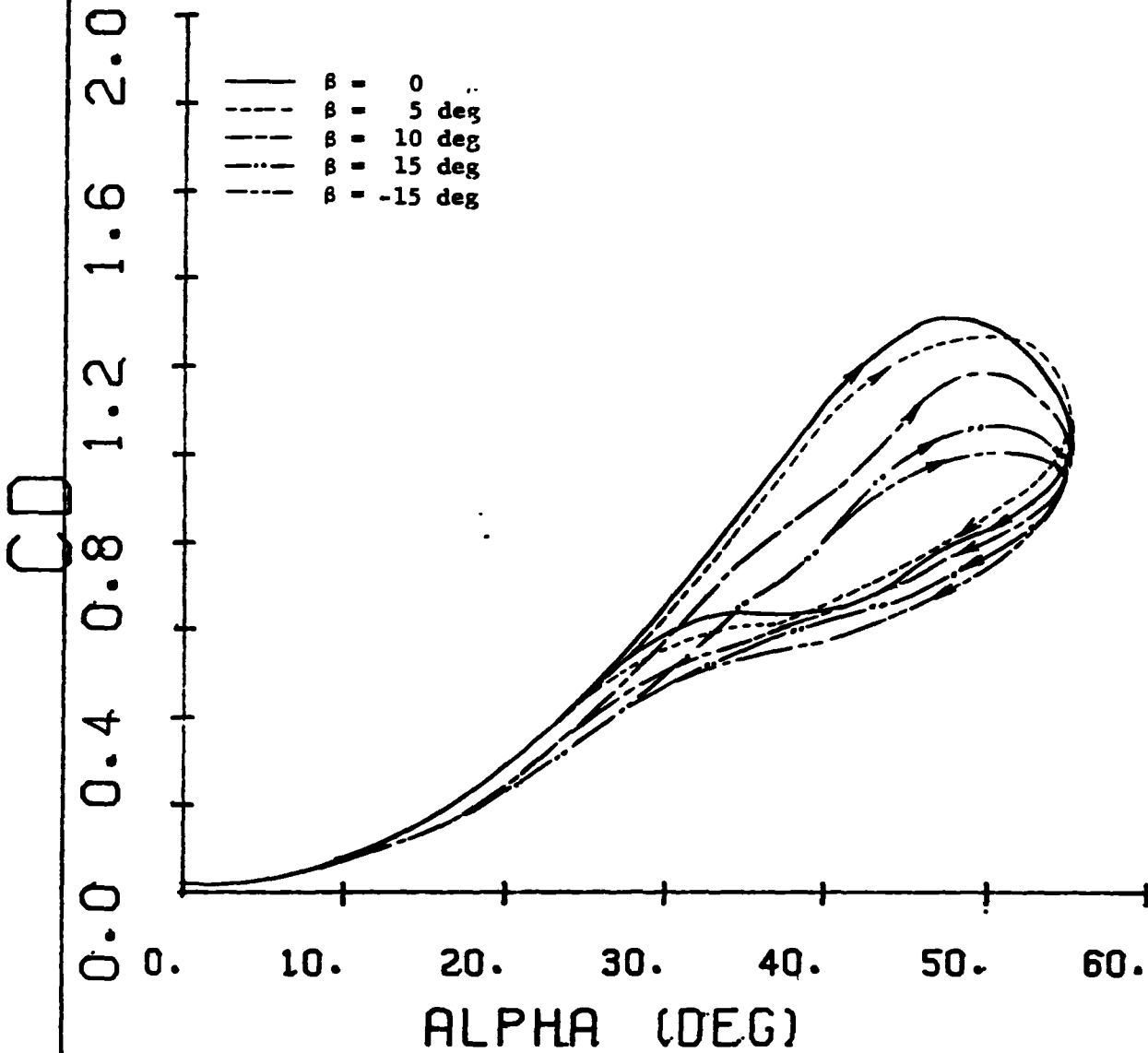


UNSTEADY AERODYNAMIC EFFECT ON PITCH MOMENT VARYING SIDESLIP ANGLE

(K = 0.043)



CD VS. ALPHA

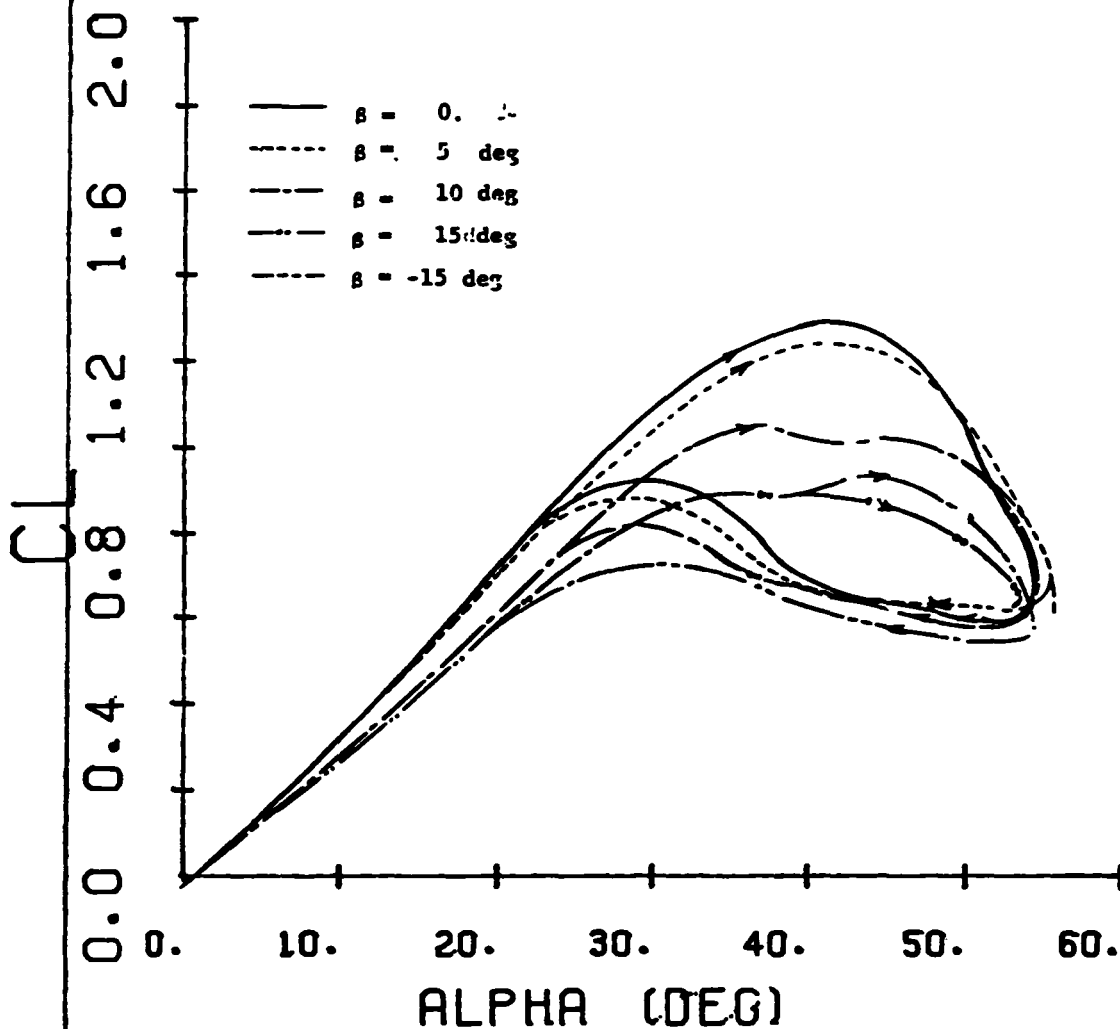


UNSTEADY AERODYNAMIC EFFECT ON DRAG VARYING SIDESLIP ANGLE

($K = 0.043$)

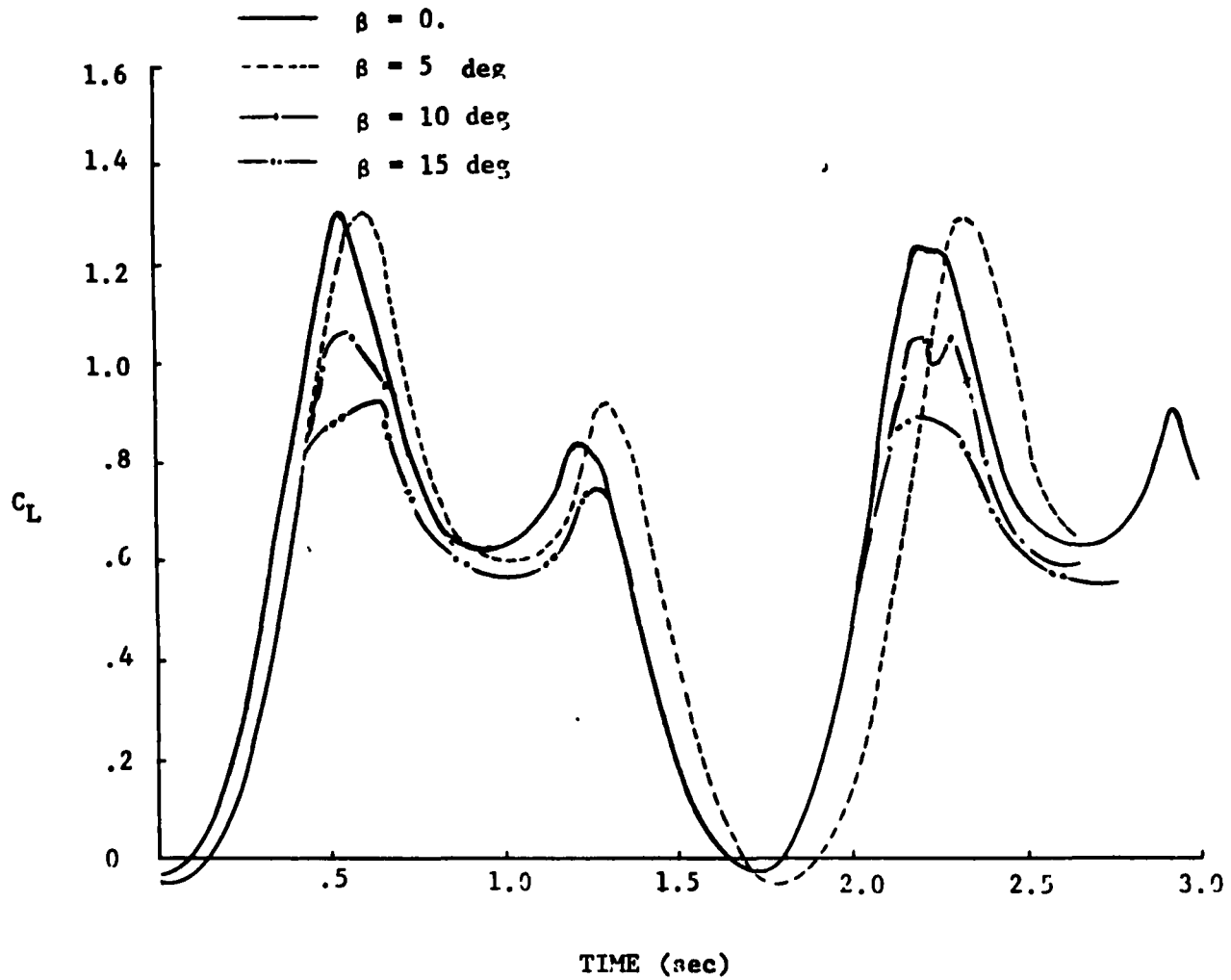
T · H · E
OHIO
STATE
UNIVERSITY

CL VS. ALPHA



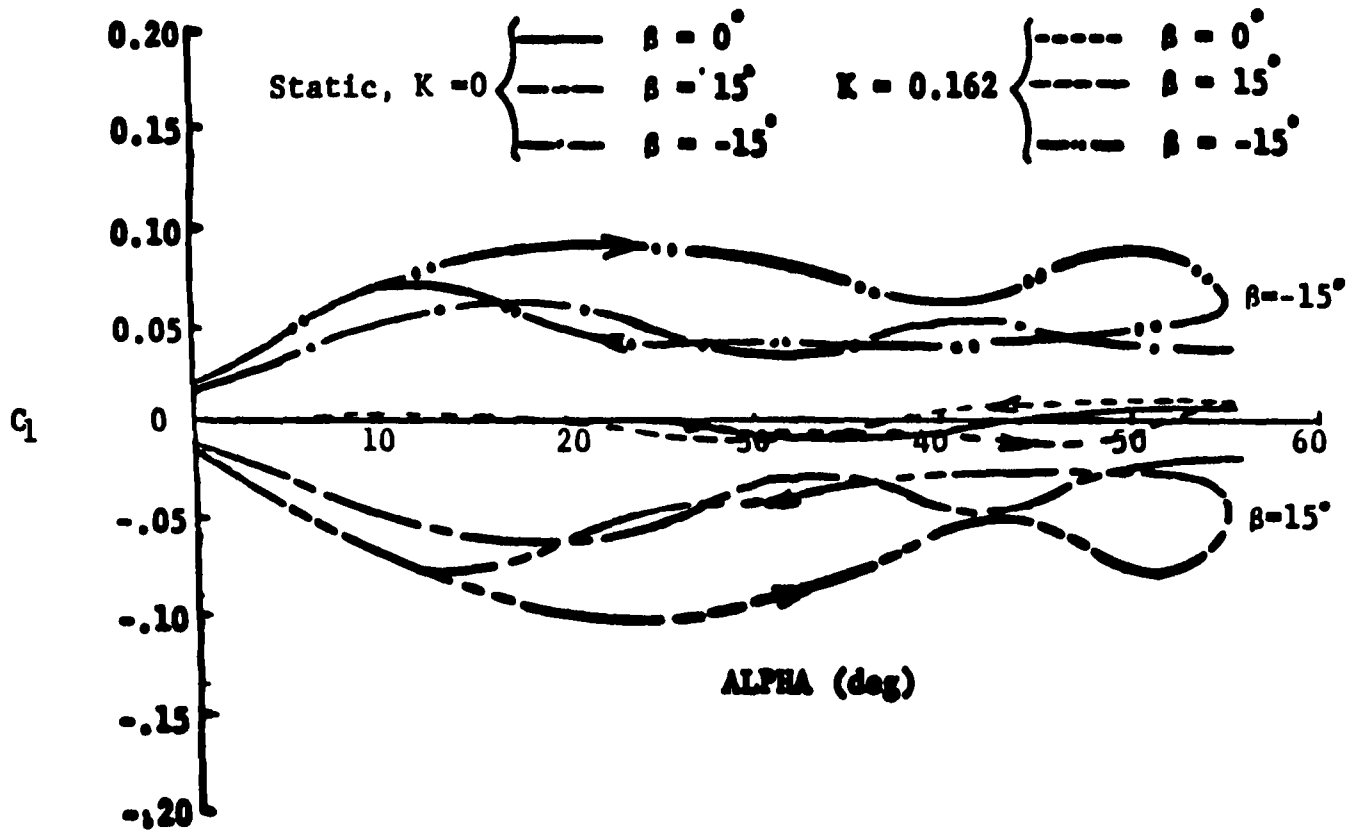
UNSTEADY AERODYNAMIC EFFECT ON LIFT VARYING SIDESLIP ANGLE
(k = 0.043)





VARIATION OF LIFT COEFFICIENT vs. TIME (sec)



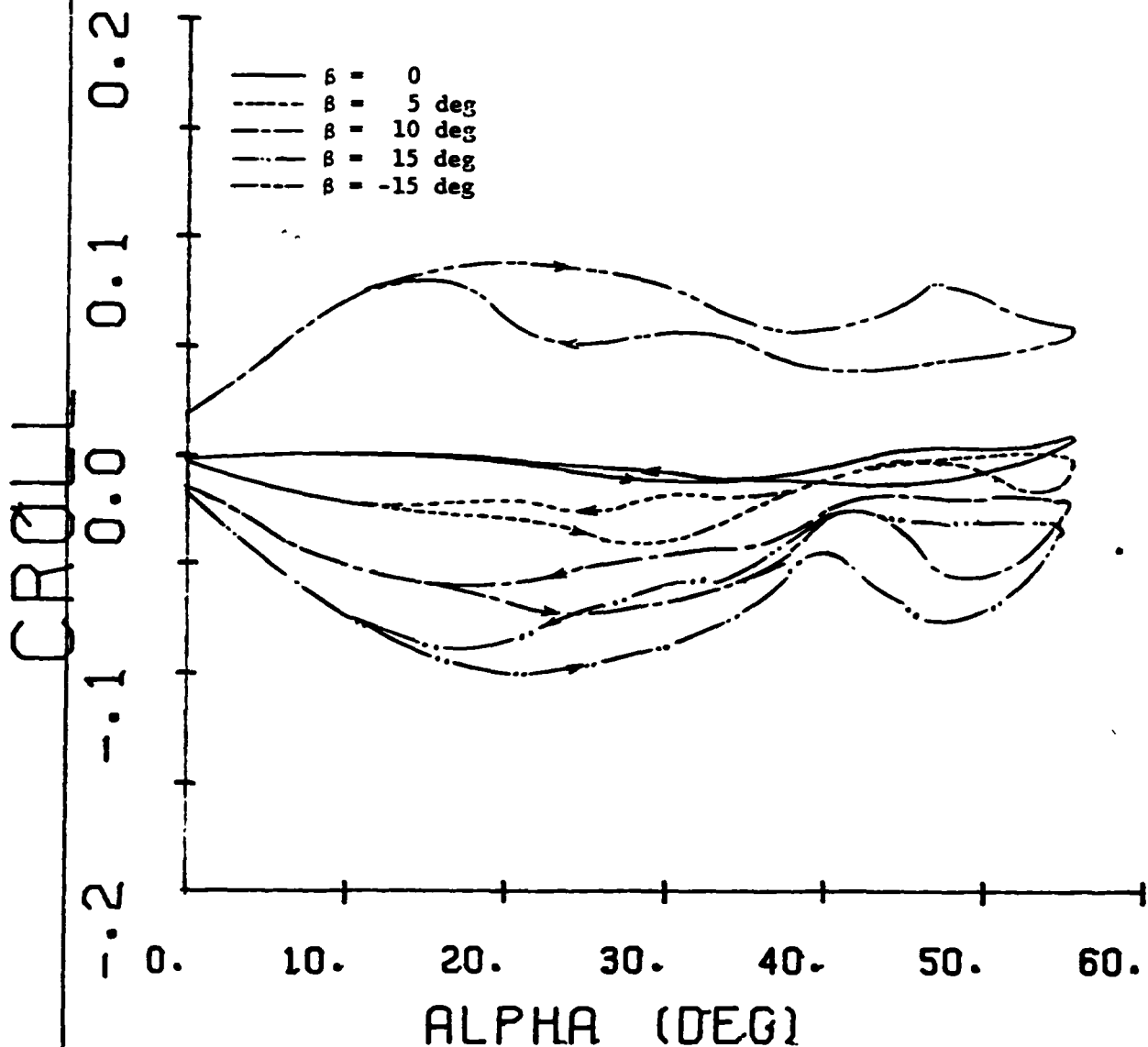


UNSTEADY AERODYNAMIC EFFECT ON ROLLING MOMENT

DELTA WING



CROLL VS. ALPHA

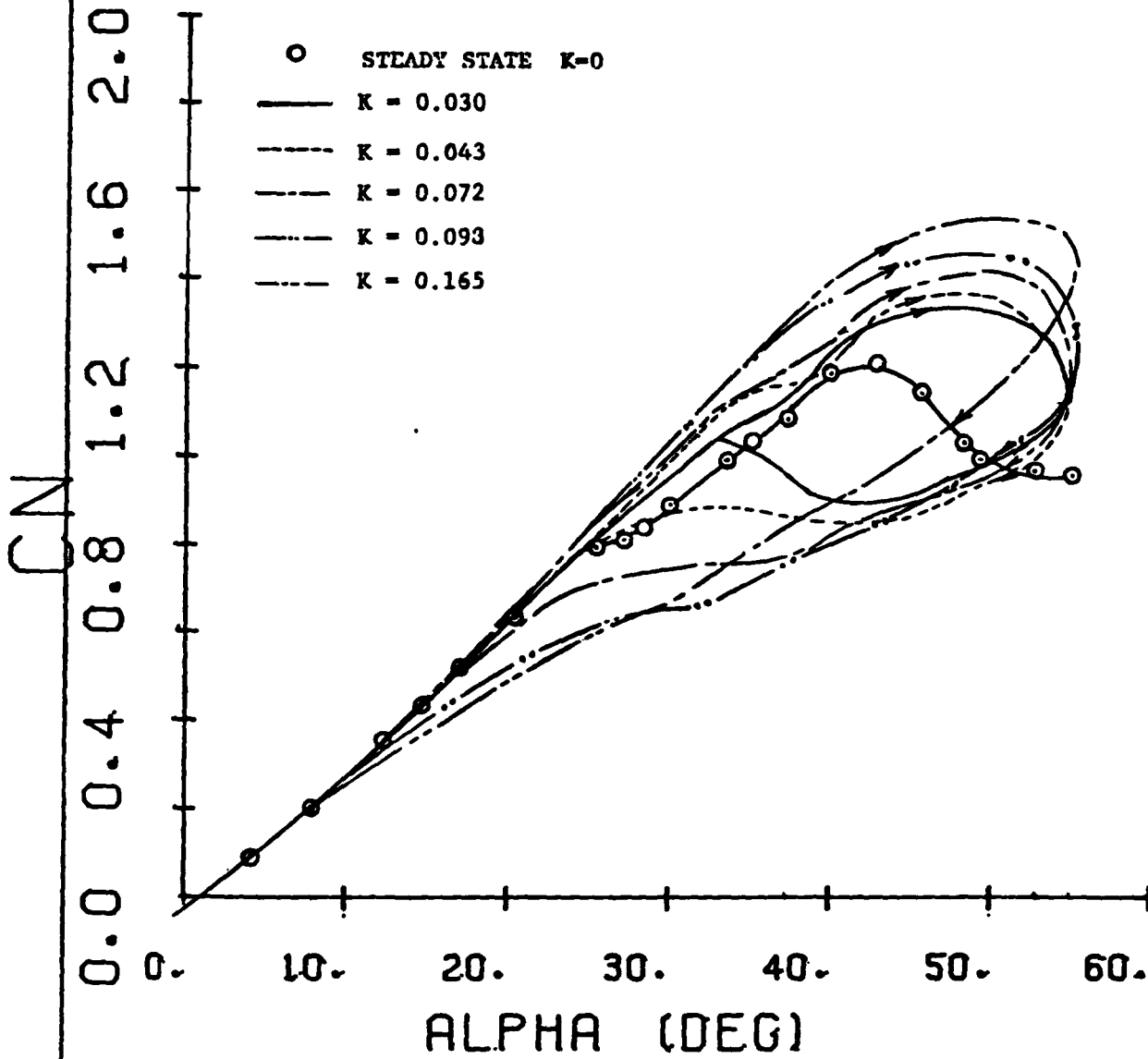


UNSTEADY AERODYNAMIC EFFECT ON ROLLING MOMENT VARYING SIDESLIP

($K = 0.043$)



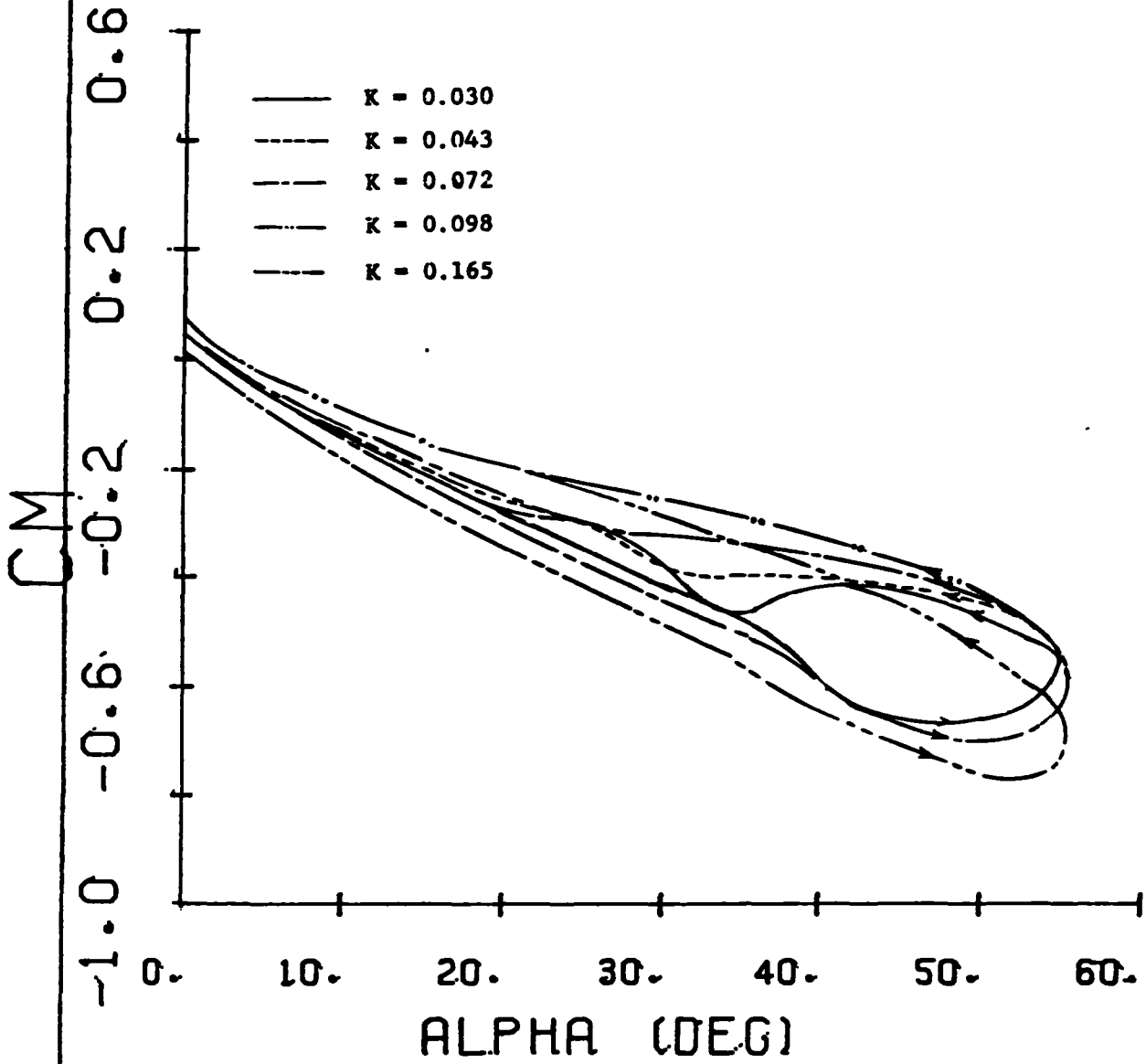
CN VS. ALPHA



UNSTEADY AERODYNAMIC EFFECT ON NORMAL FORCE ($\beta = 15$ deg)



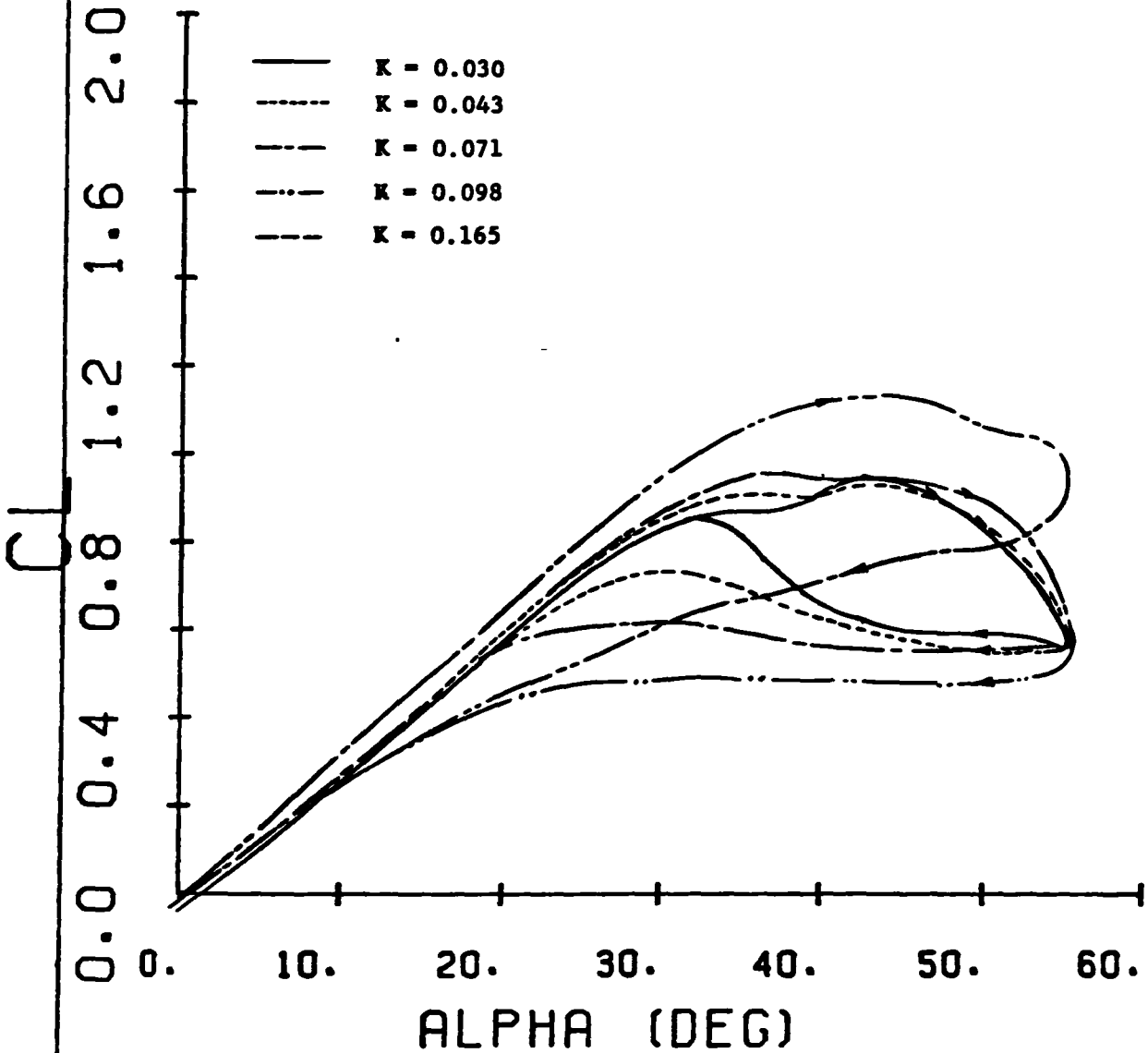
CM VS. ALPHA



UNSTEADY AERODYNAMIC EFFECT ON PITCHING MOMENT ($\beta=15$ deg)



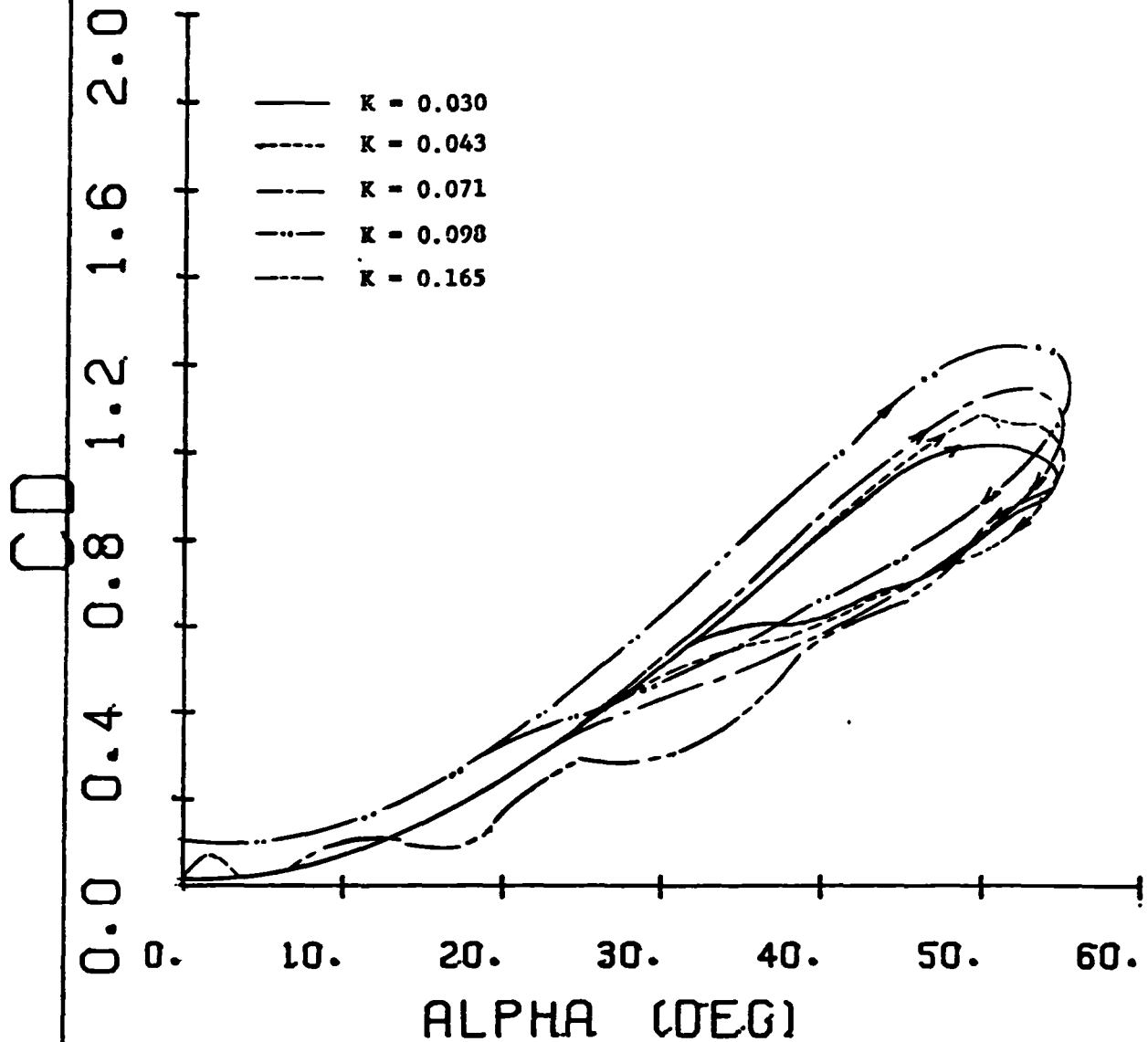
CL VS. ALPHA



UNSTEADY AERODYNAMIC EFFECT ON NORMAL FORCE ($\beta = 15$ deg)



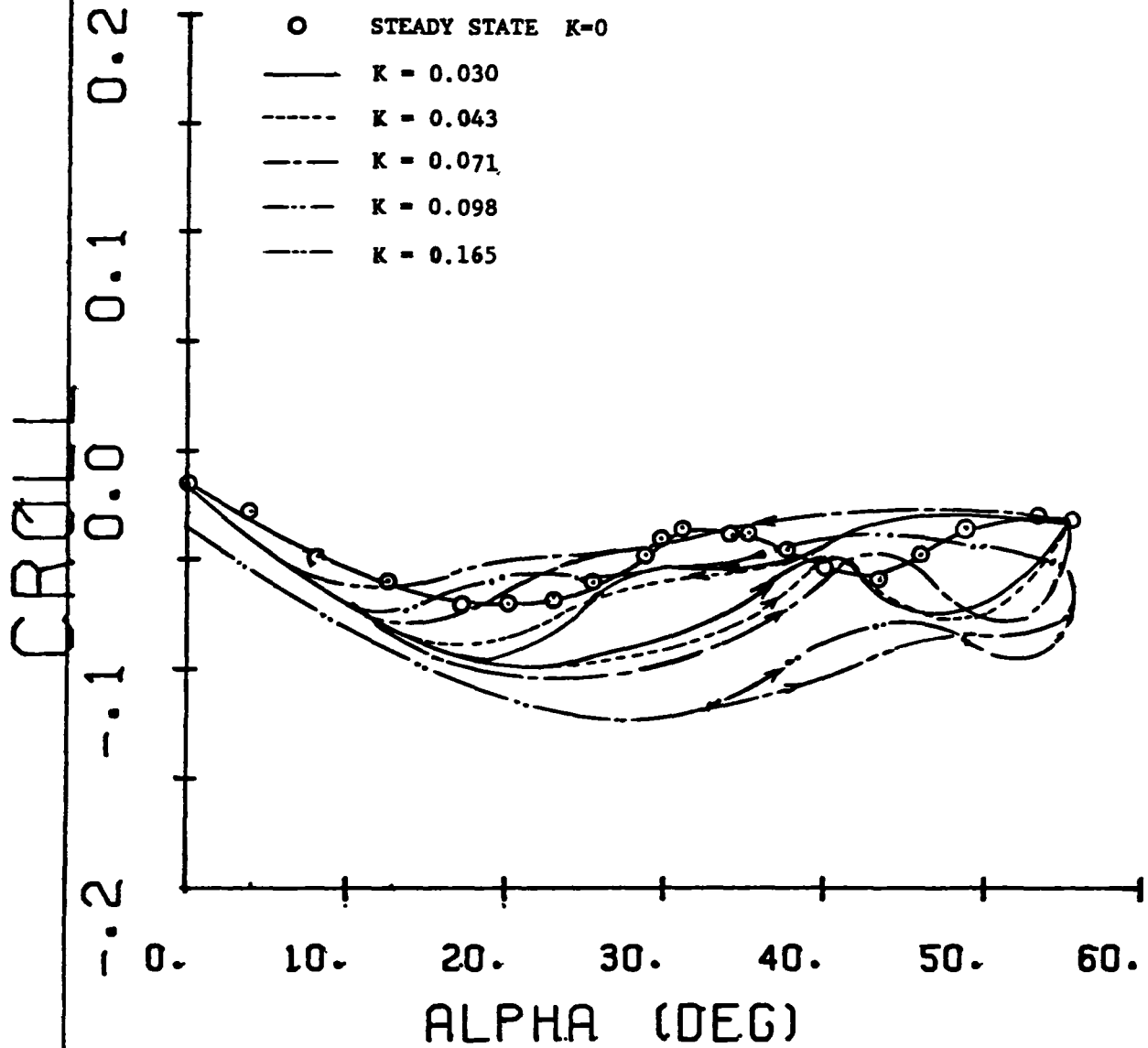
CD VS. ALPHA



UNSTEADY AERODYNAMIC EFFECT ON DRAG ($\beta = 15$ deg)



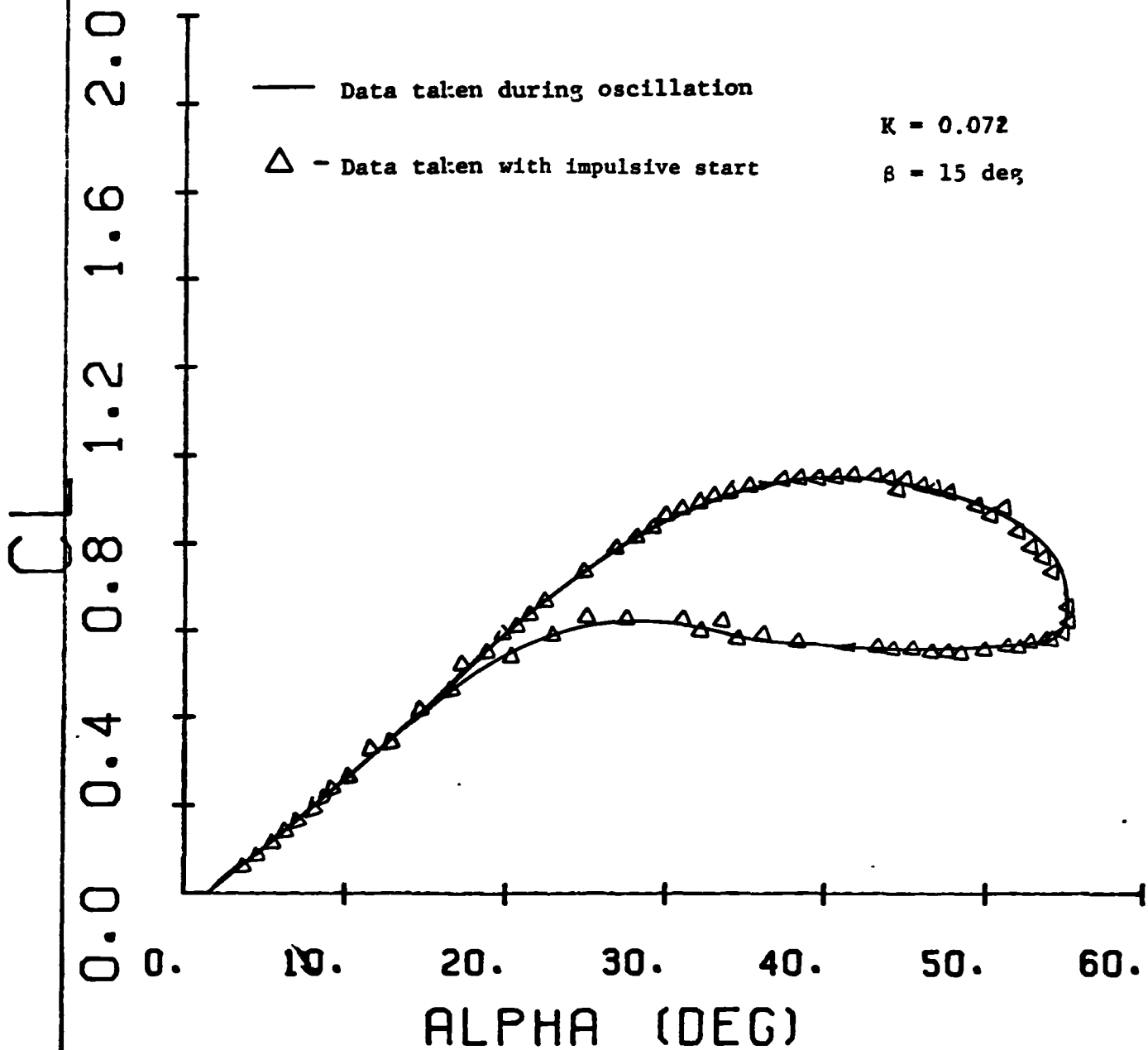
CROLL VS. ALPHA



UNSTEADY AERODYNAMIC EFFECT ON ROLLING MOMENT ($\beta=15$ deg)

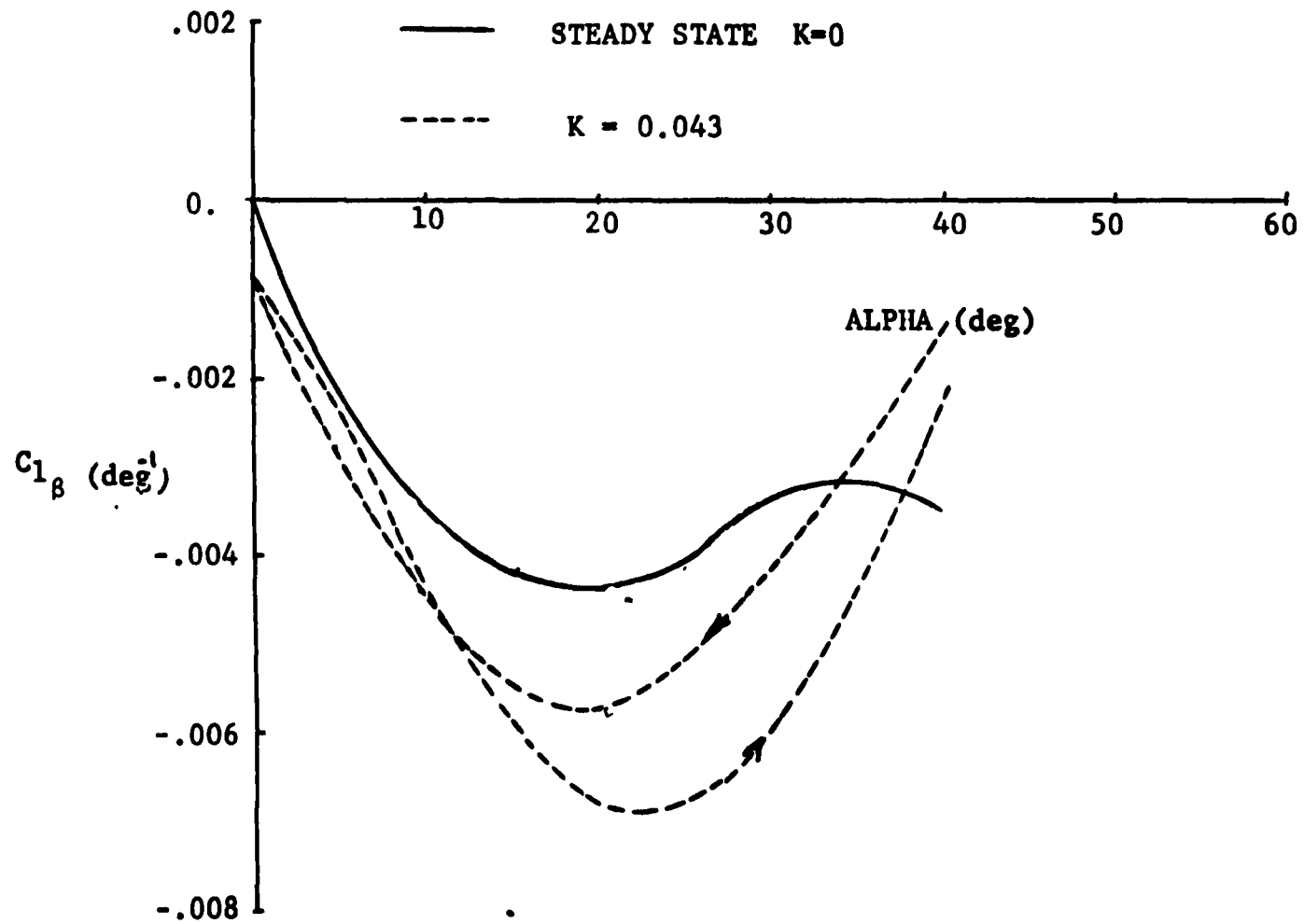


CL VS. ALPHA



EFFECTS OF IMPULSE START ON DELTA WING MODEL





DIHEDRAL EFFECT (deg⁻¹) vs ALPHA (deg)



SUMMARY

- **HARDWARE AND SOFTWARE HAVE BEEN DEVELOPED AND TESTED AT OSU TO OSCILLATE A HIGH PERFORMANCE AIRCRAFT MODEL IN SUBSONIC FLOW AND OBTAIN SIX-COMPONENT BALANCE DATA.**

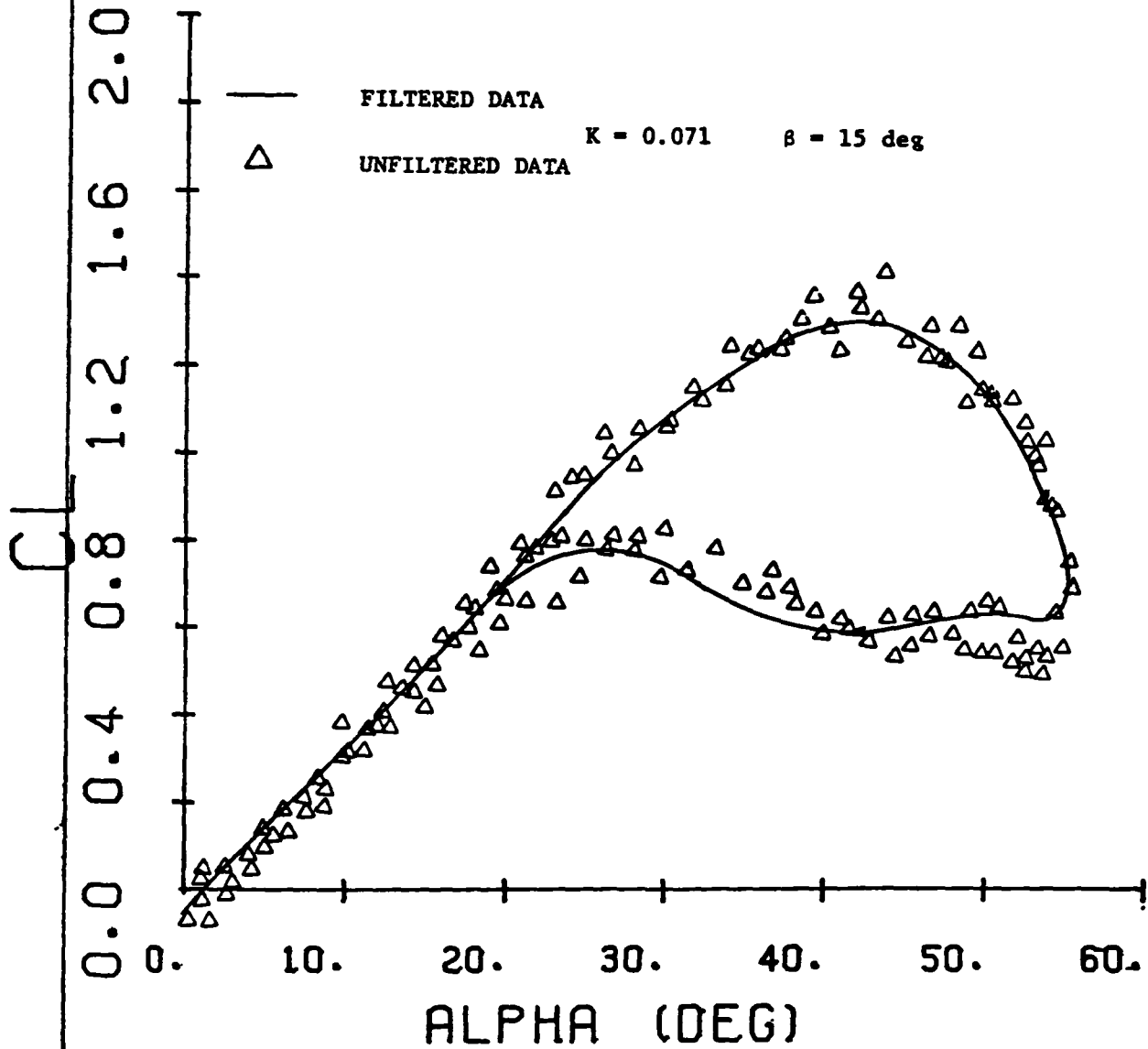
- **DATA SHOW A STRONG INFLUENCE OF PITCH RATE ON FORCES AND MOMENTS**

HYSTERESIS LOOPS ARE SEEN IN ALL OSCILLATING MODEL DATA.

MODEL OSCILLATION WITH SIDESLIP INTRODUCES NON-LINEAR ASYMMETRIC FORCES AND MOMENTS APPARENTLY DUE TO ASYMMETRIC VORTEX BURSTING.



CL VS. ALPHA



COMPARISON OF FILTERED AND UNFILTERED DATA



End of Document